Effect of Sulfate Electrolyte Additives on $LiNi_{1/3}Mn_{1/3}Co_{1/3}O_2$/graphite Pouch Cell Lifetime: Correlation between XPS Surface Studies and Electrochemical Test Results.

Journal:	*The Journal of Physical Chemistry*
Manuscript ID:	jp-2014-09731y.R1
Manuscript Type:	Article
Date Submitted by the Author:	23-Nov-2014
Complete List of Authors:	Madec, Lénaïc; Dalhousie University, Xia, Jian; Sun Yat-sen University, Petibon, Remi; Dalhousie Univ., Physics Nelson, Kathlyne; Dalhousie Univ., Physics Sun, Jon-Paul; Dalhousie University, Department of Physics Hill, Ian; Dalhousie University, Department of Physics Dahn, Jeff; Dalhousie Univ., Physics

Effect of Sulfate Electrolyte Additives on $LiNi_{1/3}Mn_{1/3}Co_{1/3}O_2$/graphite Pouch Cell Lifetime: Correlation between XPS Surface Studies and Electrochemical Test Results.

Lénaïc Madec[1], Jian Xia[1], Rémi Petibon[2], Kathlyne J. Nelson[1], Jon-Paul Sun[1], Ian G. Hill[1] and Jeff R. Dahn[1,2,]*

[1]Department of Physics and Atmospheric Science, Dalhousie University, Halifax, B3H3J5, Canada

[2]Department of Chemistry, Dalhousie University, Halifax, B3H4R2, Canada

ABSTRACT

The role of two homologous cyclic sulfate electrolyte additives, trimethylene sulfate (or 1,3,2-Dioxathiane-2,2-dioxide, TMS) and ethylene sulfate (or 1,3,2-Dioxathiolane-2,2-dioxide, DTD) used either alone or in combination with vinylene carbonate (VC) on the lifetime $LiNi_{1/3}Mn_{1/3}Co_{1/3}O_2$(NMC)/graphite pouch cells were studied by correlating data from gas

chromatography/mass spectroscopy (GC-MS), dQ/dV analysis, ultra high precision coulometry, storage experiments and X-ray photoelectron spectroscopy (XPS). For VC alone, more stable and protective SEI films were observed at the surface of both electrodes due the formation of a polymer of VC which results in higher capacity retention. For TMS, similar chemical SEI compositions were found compared to the TMS-free electrolytes. When VC was added to TMS, longer cell lifetime is attributed to VC. For DTD, a cell lifetime that competes with VC was explained by a preferential reduction potential and a much higher fraction of organic compounds in the SEI films. When VC was added to DTD, the contribution of both additives to the SEI films is consistent with the initial reactivity observed from dQ/dV and GC-MS analysis.

Keywords: XPS, $LiNi_{1/3}Mn_{1/3}Co_{1/3}O_2$/graphite, pouch cell, lifetime, sulfate additives, electrochemical test.

1. Introduction

Extending the life time of Li-ion cells to several decades, for vehicle and grid storage applications, is one of the most challenging problems for battery researchers. The use of electrolyte additives is a simple, economical and effective approach to improve both cycle and calendar life as well as cycling performance of Li-ion batteries[1,2]. During cycling and storage of a Li-ion cell, degradation of electrolyte solvents and/or salts can occur and can lead to the formation of very complex surface films at the electrolyte/electrode interfaces. The resulting so-called solid electrolyte interphases (SEI)[3] are composed of organic and inorganic species. The main role of electrolyte additives is to prevent such unwanted parasitic reactions by modifying

the SEI films. Although the chemical nature and morphology of those films have been carefully analysed during the last decade, most studies have been on common electrolytes with no additives (e.g. a mixture of carbonate solvents with $LiPF_6$ as the salt). Therefore, despite increasing numbers of studies on electrolyte additives, their exact impact on the chemistry and morphology of the SEI still remain poorly understood.

Vinylene carbonate or 1,3-Dioxol-2-one (VC), first proposed by SAFT[4], is certainly the most used and known electrolyte additive for Li-ion cells[5,6,7,8]. It has been shown to improve the electrochemical performance and thermal stability of different Li-ion systems[9,10,11,12,13]. In addition to the preferential reduction of VC that some researchers believe results in the stabilization of solvent degradation on the negative electrodes, it has also been shown that VC causes major beneficial effects on positive electrodes[6,8,10,12]. Recently, high precision coulometry[14] and storage experiments[15] have shown that VC decreases the rate of parasitic reactions (*i.e.* electrolyte oxidation) at the positive $LiCoO_2$ electrode. Electrochemical performance of VC-containing cells degrades, however, at very high voltages[16] and high temperatures[17] due to extensive electrolyte degradation. The polymerizable vinyl group in VC greatly influences its reactivity. Based on experimental and theoretical studies, various mechanisms have been proposed such as the formation of VC polymerization products as well as non-polymeric species such as lithium alkyl dicarbonate salt[6,18,19]. Recently, Ouatani *et al*. have found the deposition of a polymer of VC at the surface of both electrodes of a $LiCoO_2$/graphite cell[20]. Using XPS analysis and theoretical simulations, they proposed a radical polymerization mechanism of VC as main reaction pathway. They also showed that during the reaction of VC, no interaction occurred between the negative and positive electrodes (e.g. exchange of chemical

species from one electrode to the other) as during the first charge of a $LiFePO_4$/graphite cell, the polymeric product of VC was found only at the surface of the graphite[21] while it is observed at both electrodes for a $LiCoO_2$/graphite cell.

More recently, sulfur-containing electrolyte additives have also been the subject of numerous studies and show promising performance[22,23,24,25,26,27,28]. Ethylene sulfate or 1,3,2-Dioxathiolane-2,2-dioxide (DTD) has been used as a film forming additive to enable the use of propylene carbonate based electrolytes with graphite electrodes by preventing exfoliation[29,30]. The study done by Xia *et al*.[31] reports on the use of high precision coulometry and storage experiments to compare the effect of DTD with trimethylene sulfate or 1,3,2-Dioxathiane-2,2-dioxide (TMS), a homologous cyclic sulfate that differ only by the carbon-ring as shown in Figure 1. They found that the carbon-ring strongly influences the behaviour of these additives in $LiNi_{1/3}Mn_{1/3}Co_{1/3}$(NMC)/graphite pouch cells as DTD could compete with VC in terms of cell performance as a single additive while TMS showed little performance gain compared to the control electrolyte with no additive. The combination of VC with TMS or DTD led, however, to similar electrochemical performance compared to VC used singly which raises questions about the exact effects of these sulfur-based additives.

In the present work, the role of TMS and DTD additives used singly or in combination with VC on the electrochemical performance and the resulting lifetime of $LiNi_{1/3}Mn_{1/3}Co_{1/3}O_2$(NMC)/graphite pouch cells has been investigated. Gas chromatography coupled with electron impact mass spectroscopy (GC-MS) has been performed to understand the dQ/dV plots recorded during the early stage of the formation cycle for the different electrolyte

compositions. Coulombic inefficiency (1 – CE) as well as charge end point capacity slippage have been carefully recorded using ultra high precision charger (UHPC) experiments[32,33]. SEI films formed at both negative and positive electrodes during formation and after cycling of the cells have been thoroughly analysed by X-ray Photoelectron Spectroscopy (XPS) and have been correlated to the electrochemical differences observed between electrolytes.

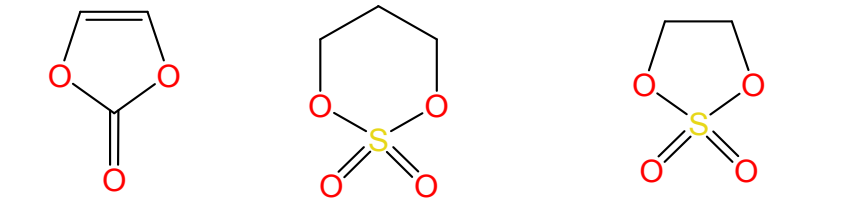

Figure 1. Molecular formula and structural information for VC, TMS and DTD.

2. Experimental

Materials and cell preparation. – Machine made 220 mAh $LiNi_{1/3}Mn_{1/3}Co_{1/3}O_2$/graphite (NMC/graphite) pouch cells were obtained dry (vacuum sealed with no electrolyte) from Li-Fun Technology (Xinma Industry Zone, Golden Dragon Road, Tianyuan District, Zhuzhou City, Hunan Province, PRC, 412000). SEM images of the top surfaces of the NMC and graphite electrodes are presented in Figure S1 so that readers can appreciate the morphology of the particles that make up the electrodes. Before electrolyte filling, the pouch cells were cut just below the heat seal and dried at 80°C under vacuum for at least 12 h to remove any residual water. Cells were then filled with 0.9 g of electrolyte in an argon-filled glove box. In this study, 1 M $LiPF_6$ (BASF, purity 99.94%, water content < 14 ppm) EC:EMC (3:7 by weight, BASF, water

content < 20 ppm) was used as the control electrolyte. To this electrolyte, 2 wt% of Vinylene carbonate (VC, BASF, purity > 99.8%, water content < 100 ppm) was added singly or in combination with either 2 wt% TMS (Aldrich, purity > 98%) or 2 wt% DTD (Aldrich, purity > 98%). The cells were then vacuum-sealed at a gauge pressure of -94 kPa (relative to atmospheric pressure) using a compact vacuum sealer (MSK-115A, MTI Corp.). For each of the following formation/cycling/storage experiments, two cells were used to confirm the reproducibility of the corresponding electrochemical tests.

Cell formation, cycling and storage protocol. – After filling, formation was performed on a Maccor 4000 series cycler as follows. Cells were placed in a temperature-controlled box at 40 ± 0.1°C and held at 1.5 V for 24 hours to allow for the completion of wetting. Cells were then charged to 3.8 V using a current of 11 mA (C/20). After this step, cells were cut open in an argon-filled glove box to release any gas generated during formation and then vacuum sealed again. Cells were then charged to 4.2 V and discharged to 2.8 V at 11 mA (C/20). Note that for each charge/discharge step during formation, pouch cells intended for the XPS study were held at the chosen potential until the measured current decreased to 0.005 C so that electrodes are supposedly in electrochemical equilibrium.

For the XPS study, cells were cycled on a Maccor 4000 series cycler between 4.2 and 2.8 V at 40.0 ± 0.1°C at 11 mA (C/20) for 23 cycles (*i.e.* 24 cycles including the formation cycle) then cells were stopped either fully charged at 4.2 V or fully discharged at 2.8 V. Pouch cells were then carefully disassembled in an argon-filled glove box within the 24 hours following the end of the formation/cycling processes. Negative graphite and positive NMC electrodes were cut from

the pouch cells electrodes with a precision punch and washed twice by immersion into 0.8 mL of EMC solvent (BASF) in a clean and dry glass vial with a mild manual agitation during 10 sec to remove the electrolyte. Electrodes were then dried at approx. 10^{-3} mbar in the antechamber of the glove box overnight then stored in sealed glass vials in the argon-filled glove box prior to the XPS analysis.

Ultra High Precision Chargers (UHPC) at Dalhousie University[32,33] were used to monitor the coulombic inefficiency and charge end point capacity slippage of NMC/graphite pouch cells between 2.8 and 4.2 V at 40.0 ± 0.1°C using a current of 11 mA (C/20) for 15 cycles where comparisons were made.

Additional long term cycling was also performed in order to evaluate the expected cycle life. For this purpose, NMC/graphite pouch cells were cycled on a Neware BTS3000 system between 2.8 and 4.2 V at 80 mA (C/2.5) at 55.0 ± 0.1°C.

For storage, cells were first charged with a Maccor series 4000 cycler to 4.2 V at a current of 11 mA (C/20) then held at 4.2 V until the measured current decreased to 0.0025 C. After the pre-cycling process, cells were carefully moved to the storage system which automatically monitored their open circuit voltage every 6 hours for a total storage time of 500 h [34].

Gas chromatography coupled with electron impact mass spectroscopy (GC-MS) – The procedure for the extraction of electrolyte components for GC-MS analysis followed the one previously described by Petibon *et al.*[35]. This simple method allows salts such as $LiPF_6$, which might

damage the GC column, to be removed. Prior to GC-MS analysis, pouch cells were first discharged to an open circuit potential near 0.0 V and opened rapidly outside the glove box. The jelly roll was then immediately put in a perfluoroalkoxy polymer (PFA) vial containing 10 mL of dichloromethane. The vial was then shaken automatically for 15–20 min to extract the electrolyte from the jelly roll. The supernatant was then filtered using a syringe filter with a PTFE membrane and 0.2–0.45 μm pores. A few drops of the filtrate were then added to a vial containing 10 mL of dichloromethane and 0.25 mL of distilled water, shaken for 5–10 min and centrifuged at 300 g-force for 10–15 min to eliminate any potential emulsion. The organic layer (the lower layer) was then injected in the GC-MS. The exact volume and weight of filtrate added were not measured. The results presented in this article are the weight percent of the additive relative to the total mass of EC, EMC, the additive initially introduced in the cell and other chemicals known to form through transesterification reactions such as DEC, DMC, DMOHC and DEOHC[35]. The GC-MS used was a Bruker 436-GC equipped with a split/splitless injector and a BR-5MS 30 m column with an inner diameter of 0.25 mm and a coating thickness of 1 μm. Helium was used as carrier gas at a constant flow rate of 1.3 mL/min. The GC was coupled to a Bruker Scion single-quadrupole mass spectrometer equipped with an electron impact ionization module. The injector temperature was set to 270°C and the oven temperature was programmed to get the best component separation in the shortest amount of time. The end of the oven temperature cycle was set to a 290°C for 5 min to ensure the elution of heavier highly retained compounds (mostly compounds coming from septum and column bleed). The transfer line was set to 270°C, the ion source to 270°C and the electron energy to 70 eV. The mass spectrometer was set to a single ion monitoring mode (SIM) for the measurement of EC, EMC, DMC, DEC, VC, TMS, DTD and known by-products of the dimerization of EC with either EMC, DMC, or

DEC, DMC, DEC, and the by-products of the dimerization were monitored in the eventuality that they would form during formation. After the SIM mode measurements, all solutions were measured again with the MS set to a full scan mode to verify that no other compound was present. Calibration solutions were made for quantitative analysis of electrolyte components. The calibration solutions were made by diluting known amounts of electrolyte solvents and additives in CH_2Cl_2. A minimum of five solutions of known concentration were used to obtain an external calibration curve with a squared correlation coefficient of at least 0.999.

X-ray Photoelectron Spectroscopy (XPS). – XPS was performed on a SPECS spectrometer equipped with a Phoibos 150 hemispherical energy analyzer and using Mg Kα radiation (hv = 1253.6 eV). To avoid moisture/air exposure of electrode samples during transfer from the argon-filled glove box to the spectrometer, careful precautions were taken by using a special transfer system built at Dalhousie University as presented in Figures 2a and b. This system contains a magnetic manipulator attached to a sample holder, a gate valve and a flange that fits the entry port of the spectrometer. Additionally, the transfer system can be placed under vacuum via a needle valve while the vacuum level can be monitored by a vacuum gauge. The sample transfer protocol was performed as follows. In an argon-filled glove box, electrode samples were mounted onto a molybdenum holder using a copper conductive tape (3M) and placed into the transfer system. The latter was then put under vacuum at a pressure of approx. 10^{-3} mbar during 1 hour. No significant pressure change was observed when the transfer system was left without sample under static vacuum at ~10^{-3} mbar for 1 night demonstrating the transfer system was leak free. Once evacuated, the transfer system was connected to the XPS system (Figure 2b) and samples were loaded in the load lock of the spectrometer under a pressure of ~10^{-3} mbar. Finally

all samples were kept under a pressure of 10^{-8} mbar for one night before analysis to allow a strictly identical vacuum procedure. Figures 2c and d show photographs of lithiated graphite electrodes from two different pouch cells charged at 4.2 V and loaded into the load lock and the analysis chamber of the XPS spectrometer respectively. The photos were taken through glass viewports. The gold color that corresponds to the fully lithiated state of the graphite demonstrates the reliability of the electrode sample preparation and transfer protocol. Please note that lithiated graphite samples exposed to the humid air of our laboratory lose their gold color within a few seconds.

Sample analysis using XPS was performed as follows. The operating pressure was kept below 2 x 10^{-9} mbar. The analyzed sample area was ~ 2 x 3 mm^2 which gives results representative of the whole electrode. Core spectra were recorded in the fixed analyser transmission (FAT) mode with a pass energy of 20 eV. To verify that no sample degradation occurred during analysis, short acquisition time spectra were first recorded as a reference. Data treatment was performed using CasaXPS software . The binding energy scale was calibrated from the C1s peak at 285 eV (C-C/C-H) and the O1s peak at 529.6 eV (O^{2-} anion from the $LiNi_{1/3}Mn_{1/3}Co_{1/3}$ active material) for negative graphite and positive NMC electrodes respectively. Core peak analysis was performed using a nonlinear Shirley-type background[36]. The peak positions and areas were optimized using 70% Gaussian - 30% Lorentzian Voigt peak shapes and full width at half-maximum (fwhm) constraint ranges. The following fitting procedure was then followed. A minimum number of peaks were used for the core level spectra of electrodes taken from the control cells (with no additives). When additives were used, an equal number of peaks were chosen as a first assumption and their positions were kept identical using a position constraint of ± 0.2 eV. Then,

based on the residual spectra as well as the difference spectra, additional peaks were added when clearly necessary. If additional peak(s) were needed, the position constraint was then modified to ± 0.5 eV to allow a more accurate fitting. In that case, if a significant peak shift (≥ 0.3 eV) was observed, this peak shift was considered as reliable and therefore kept only if an identical peak shift was also observed for each other electrode samples for a given additive blend. In the different figures, core level spectra of graphite electrodes were maximized to show low intensity peaks while core level spectra of NMC electrodes were normalized to show the same intensity range. The reproducibility of XPS spectra and quantification was confirmed on six sets of pair pouch cells over 30 different sets analyzed in total in the present study.

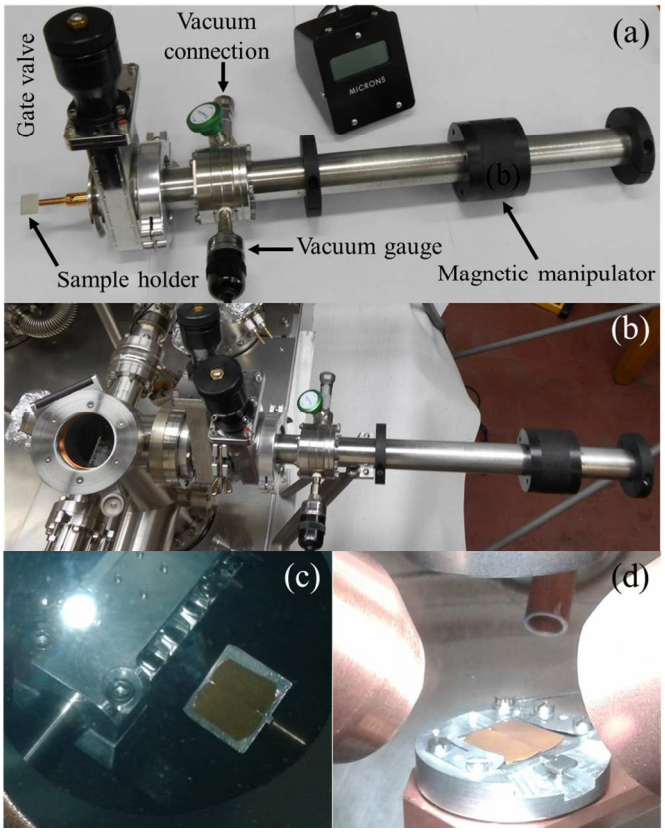

Figure 2. (a) Transfer system used at Dalhousie University; (b) a photograph of the transfer system when connected to the XPS system; (c) and (d) photographs of two lithiated (gold)

graphite electrodes charged at 4.2V in the load lock and in the analysis chamber of the XPS spectrometer, respectively.

3. Results and discussion

3.1 Electrochemical performance

Figures 3a and b show the differential capacity (dQ/dV) vs. V curves of NMC/graphite pouch cells at the beginning of the formation cycle (first cycle) with TMS and DTD-containing electrolytes, respectively. These plots allow a better determination at which cell terminal voltage the additives initially react with the lithiated graphite. For control electrolyte, a pronounced peak is observed at 2.75 V (graphite at ~ 0.8 V vs. Li/Li^+) and is attributed to the preferential reduction of EC[37,38]. When 2% VC is used, this peak becomes barely visible and a peak at a lower cell terminal voltage of ~ 2.6 V (graphite at ~ 0.9 V vs. Li/Li^+) appears. This latter peak is assigned to the lower reduction potential of VC[20] which is consistent with the consumption of VC observed by GC-MS (Figure 4a)[35]. The results in Figure 4a suggest that VC greatly reduced the electrochemical degradation of EC.

VC also prevents the transesterification of EMC into DEC and DMC (Figure 4c) compared to control electrolyte for which about 50% of EMC is converted after 1 full cycle, in agreement with a previous study[35]. Additionally, the dimerization of EC with EMC, DEC and DMC that accounts for 1-3% of the total electrolyte weight in the case of the control cells is nearly supressed (< 0.1%) when VC is used, as previously reported[35]. Figure 3a shows that for cells with TMS, only one peak appears near 2.7 V (graphite ~ 0.9 V vs. Li/Li^+). It is suggested that

this peak arises from both an electrochemical reaction of TMS and the expected reduction of EC at this potential[37,38]. This assumption is supported by the consumption of ~ 40% of TMS after formation at 3.8 V (Figure 4b). Moreover, when TMS is used singly, the amount of transesterification of EMC into DEC and DMC is similar compared to control electrolyte (Figure 4b). The dimerization of EC with EMC, DEC and DMC is in the range of 1-3 wt% of electrolyte as for the control cells. This result suggests that TMS may have almost no impact on the degradation process of the carbonate solvents.

When VC is added to TMS (Figure 3a), the peak at 2.7 V is almost suppressed and a small peak near 2.5 V is observed. This peak is attributed to the reaction of VC and has a similar intensity as VC used singly, in good agreement with the similar consumption of VC compared to VC used singly as detected by GC-MS (Figure 4a). It is therefore more likely that VC decreases both the degradation of EC and TMS. GC-MS analysis supports this hypothesis as only 20% of TMS is consumed when VC is added compared to 40% for TMS used singly. There was almost no transesterification of EMC when VC was added to TMS and the dimerization of EC with EMC, DEC and DMC was reduced to less than 0.1 wt% of electrolyte.

Figure 3b shows that for cells with DTD, two peaks are present near 2.35 and 2.7 V (graphite at 1.25 and 0.8 V vs. Li/Li^+ respectively). The first peak at 2.35 V is assigned to the electrochemical reaction of DTD in agreement with the consumption of about 60% of DTD as measured by GC-MS (Figure 4b). Note that DTD appears to react more and at a lower potential than TMS which may result in a greater beneficial effect. For instance, the second peak at 2.7 V is attributed to a lower reduction of EC compared to control and TMS electrolytes. Although VC

has slightly more impact, the transesterification of EMC is significantly decreased by DTD compared to control and TMS electrolytes (Figure 4c) and the dimerization of EC is also low (< 0.1 wt% of electrolyte). When DTD is used in combination with VC, the peak previously assigned to DTD at 2.35 V slightly decreases which is explained by a slightly lower consumption of DTD as shown by GC-MS (Figure 4b). The peak at 2.7 V, due to the reduction of EC is almost replaced by a peak at 2.6 V assigned to VC. This latter peak, however, has about half the intensity of the peak at 2.6 V observed for VC used singly. It suggests that when DTD is added to VC, DTD reacts first in a similar amount as DTD used singly and then this reduces the reactivity of VC by half. This is fairly consistent with 50% lower consumption of VC when VC + DTD is used compared to VC only. (Figure 4a). Note that the transesterification of EMC is further reduced due to the addition of VC to DTD (Figure 4c).

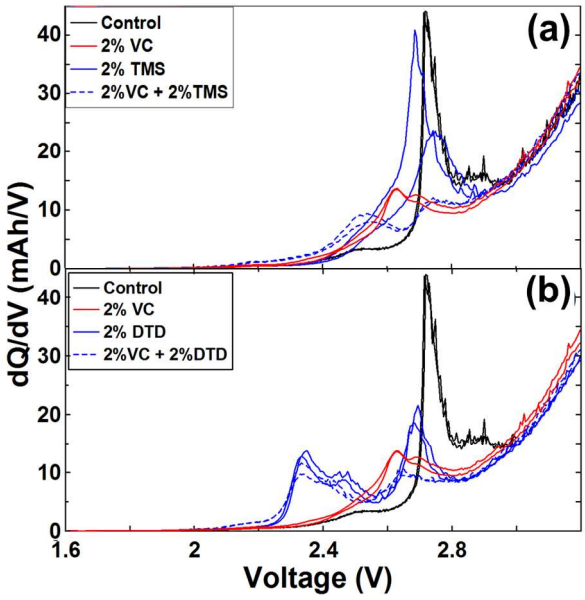

Figure 3. Differential capacity (dQ/dV) versus voltage (V) during the early stage of the formation cycle of the NMC/graphite pouch cells at C/20 and 40°C for (a) TMS and (b) DTD containing electrolytes.

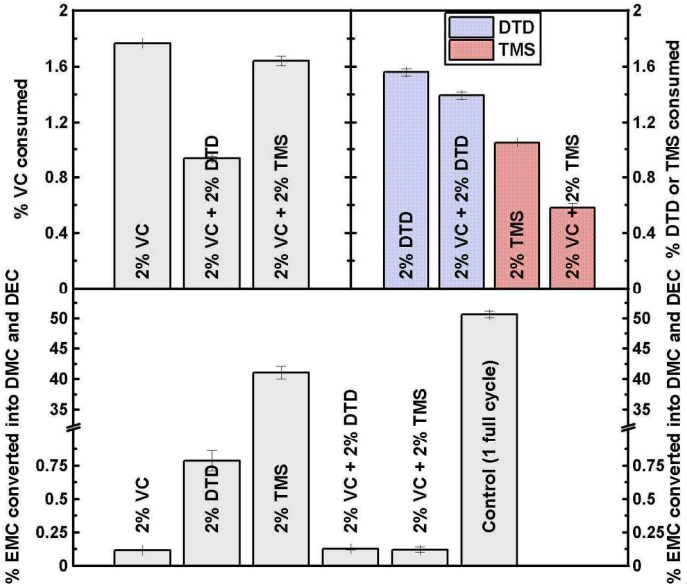

Figure 4. Amount of (a) VC, (b) TMS and DTD consumed in NMC/graphite pouch cells after formation at 3.8 V. (c) Amount of EMC converted into DMC and DEC in NMC/graphite pouch cells after formation at 3.8 V.

Figures 5a, 5b and 5c show a summary of the coulombic inefficiency (1 – CE), charge end point capacity slippage rate (Ch. Slip. in mAh/cycle) and voltage drop during storage (V_{drop}) of the NMC/graphite pouch cells studied here. The CIE was calculated from the CE taken as an average of the final three data points (cycles 13–15) collected on the UHPC. The charge end point capacity slippage rate was calculated from the slope of a best fit line to the final five points (cycles 11–15) of the charge end point capacity versus cycle number curve. As recently demonstrated by Burns et al.[39,40] the short-term CIE and charge slippage can be used to rank cells by their projected lifetime. Figures 5a, 5b and 5c show that only DTD as a single additive can provide similar performances to VC in CIE, charge end point capacity slippage and voltage drop during storage, while TMS gives results that lie between control and VC. When VC is used in

combination with DTD or TMS, properties are slightly improved compared to VC as single additive.

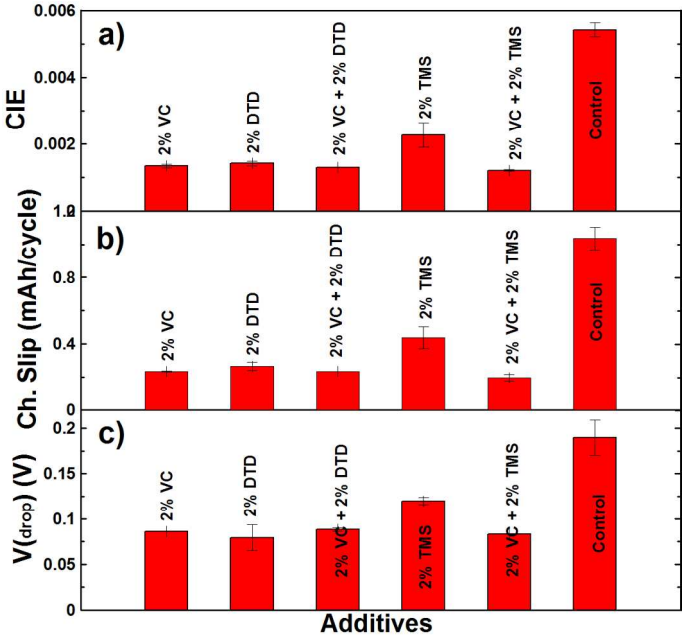

Figure 5. Summary of the high precision cycling and storage data for the NMC/graphite pouch cells: (a) coulombic inefficiency (CIE) during cycling; (b) charge end point capacity slippage during cycling; and (c) voltage drop during storage.

Figure 6 shows the discharge capacity versus cycle number collected for NMC/graphite pouch cells with electrolytes containing VC, TMS or DTD as well as VC + TMS and VC + DTD. Although the discharge capacity over the short term is well maintained for all cells (Figure 6a), some trends can be observed. Cells with control electrolyte clearly show higher discharge capacity fade as expected due to their poor rankings in Figure 5. When 2% VC was added, the discharge capacity retention was greatly improved which is consistent with the high precision coulometry data (Figure 5). When TMS was used singly, the discharge capacity showed an

intermediate fade compared to control and VC electrolytes due to its intermediate electrochemical performance (Figure 5). The use of 2% DTD lead to a slightly better discharge capacity retention than VC since DTD was found to compete well with VC in the characterizations summarized by Figure 5. When TMS or DTD were used in combination to VC, a slightly better capacity retention compared to DTD alone or VC alone was observed in agreement with the high precision coulometry data (Figure 5). Figure 6b shows the results of long term cycling at 55°C and C/2.5 between 2.8 and 4.2 V. When VC alone was used, the discharge capacity retention is greatly enhanced compared to control electrolyte for which the initial capacity falls below 80% after only 110 cycles. For cells with both TMS and DTD used in combination with VC, lower capacity fade rates were observed up to 550 cycles compared to VC. Beyond 550 cycles, however, the capacities of cells with 2% VC + 2% TMS started to decrease more quickly than cells with 2% VC electrolyte. Both sulfur-based additives used in combination with VC reached 80% of the initial 220 mAh capacity after 750 cycles compared to 650 cycles for VC. This result indicates a beneficial effect of these sulfur-containing additives in agreement with the short term UHPC cycling which was measured at 40^{o}C. Surprisingly, in the case of DTD used alone, the capacity fell very quickly after only 150 cycles. It is therefore suggested that DTD forms a SEI film that is not stable enough for long term cycling at 55°C.

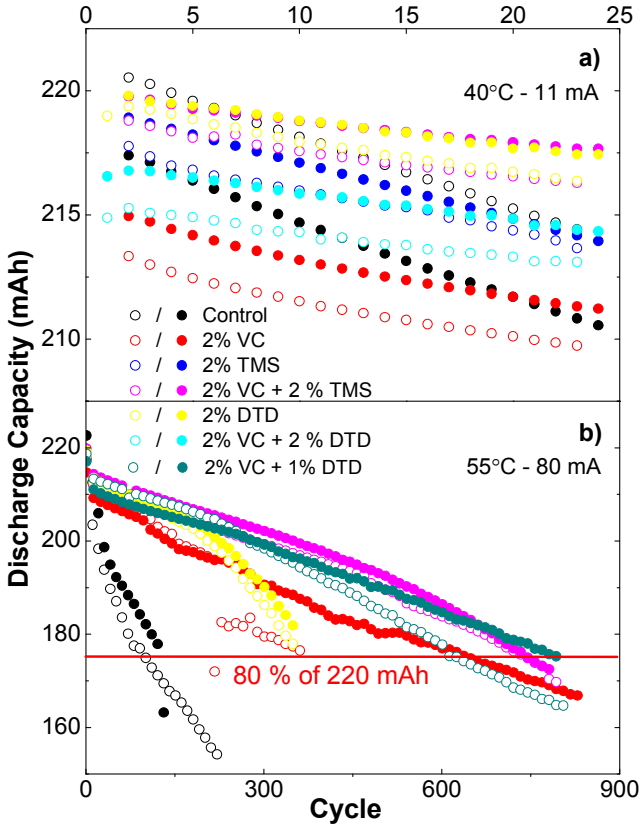

Figure 6. Discharge capacity versus cycle number for NMC/graphite pouch cells (220 mAh) with different electrolyte additives as indicated when cycled between 2.8 and 4.2 V at (a) 40.0 ± 0.1°C and a current of 11 mA (C/20) and (b) 55 ± 0.1°C and a current of 80 mA (C/2.5).

3.2 XPS analysis for VC as additive

Our aim is to understand and compare the impact of TMS and DTD additives on the electrode/electrolyte interfaces and learn how those interfaces are correlated to the corresponding electrochemical performance. As these additives are used singly or in addition with VC, it is necessary to characterize the nature of the SEI when VC is used as a single additive compared to control electrolyte (*i.e.* without additive). The impact of the different electrolyte blends on the SEI have been studied by XPS both during formation (*i.e.* during the first cycle - at 3.8 and 4.2 V

in charge and 2.8 V in discharge) and after cycling (at 4.2 V in charge and 2.8 V in discharge, referred in the different figures to as C4.2V and D2.8V respectively) at C/20 and 40°C.

Graphite negative electrodes.

Figure 7 shows the C1s and O1s core spectra of the negative graphite electrodes for cells that used control and 2% VC electrolytes as a function of voltage and cycle number. The C1s spectrum of the fresh electrode (*i.e.* without electrolyte) shows five components. The first C1s peak at 284.3 eV corresponds to C=C from the graphite[41,42] while the second one at 285 eV is attributed to C-C/C-H from the SBR binder. The components at 286.9, 288.6 and 291 eV can be assigned to C=O, COOR carbons and the ''shake up'' satellite of graphite respectively[41,42]. During the first charge, for both control and 2% VC electrolyte, an important decrease of the magnitude of the graphite peak is observed, indicating the formation of a SEI film at the electrode/electrolyte interface which covers the underlying graphite. Compared to the fresh electrode, the graphite peak shows an important shift during charge due to the lithiation of the graphite. After discharge, this shift is still observed and can be explained by the presence of some remaining intercalated lithium into the graphite. At the end of charge, although the SEI thickness has been reported to be thinner in the presence of VC[20,21], no difference was found in the present study between control and VC electrolyte. After discharge to 2.8 V, for control electrolyte, the graphite component is partially recovered (*i.e*. the SEI thickness decreases) due to dissolution/consumption of SEI species while for 2% VC electrolyte, no change is noticed. This result means that during formation, VC electrolyte produces a more stable (from a thickness perspective anyway) SEI compared to control electrolyte. After cycling, for both control and 2%

VC electrolytes, the graphite peak has totally disappeared which denotes that the SEI thickness has increased with cycling and became higher than the 5-10 nm sampling depth measured by XPS.

The C1s spectra of these electrodes also show interesting features in the 286 - 292 eV range. Electrodes cycled in both control and VC electrolytes show the appearance of CO- and CO_2-like carbon environments at 287 and 288.6 eV respectively. These peaks are in agreement with the formation of carbonaceous species (*i.e*. degradation products of EC and/or EMC) at the surface of the graphite. However, no clear evolution in peak intensity with state of charge could be discerned. More importantly, when VC is used, two new components appear at 287.9 and 291.3 eV with a 2:1 ratio and are attributed to degradation products of VC formed electrochemically during the early stages of the formation (see the dQ/dV curve on Figure 3). More precisely, these two peaks are assigned to an oligomer of VC (called Oligo-VC hereafter) in agreement with the peak position and ratio observed recently by Ouatani *et al*. at the surface of the graphite electrode after formation of a $LiCoO_2$/graphite cell at 3 V in pure VC[20]. Note that in an earlier study, Ota *et al*. observed an additional peak in the C1s spectra of graphite electrodes at a very high binding energy of 291.8 eV when VC was used and also assigned this peak to a polymer of VC[18].

In the O1s core spectrum of the fresh electrode (Figure 7), the two observed components at 531.5 and 533.3 eV are assigned to the two oxygen atoms of the CMC binder. When control electrolyte is used (Figure 7a), these latter are replaced by two new main features at 532 and 533.8 eV which can be explained by the covering of the CMC binder at the same time as the graphite as recently proposed by Ouatani *et al*.[20]. In the case of 2% VC electrolyte (Figure 7b), the peak at 533.8 eV is slightly shifted to 533.5 eV and may result from a specific reactivity of VC toward the electrode material as discussed later. The peak at 532 eV is assigned to CO_2-like oxygen

from carbonate compounds such as lithium ethylene dicarbonate $(CH_2OCO_2Li)_2$ (LEDC)[43,44] and/or other lithium alkyl carbonates ($ROCO_2Li$) while the peak at 533.5-533.8 eV is attributed to the C-O linkages from $ROCO_2Li$ and/or polyethers[45,46]. More details about the corresponding multi-step degradation mechanisms of carbonate-based electrolytes can be found in the literature[47,48,49].

For both control and VC electrolytes, two additional peaks are observed at 530.7 and 528.6 eV and attributed to the formation of lithium alkoxide (ROLi) and lithium oxide (Li_2O) respectively[50,51]. For the lithium alkoxide peak, no correlation between the state of charge and/or electrolyte used was detected. Although the lithium oxide might arise from water according to $H_2O + 2\ Li^+ + 2\ e^- \rightarrow Li_2O\ (s) + H_2\ (g)$, in the present case, its formation from further reduction of carbonate degradation compounds is more likely[46,52]. During the formation process, Li_2O is formed during charge and presumably consumed during discharge as the intensity changes accordingly. This phenomenon is also observed after cycling indicating that the SEI changes with state of charge even after 24 cycles. During charge the amount of Li_2O increases simultaneously with the SEI thickness (as previously observed from the evolution of the C1s graphite peak), therefore Li_2O is most likely located at the outermost surface of the SEI in the present case contrary to almost all reports in the literature[46,53]. These results suggest that for control cells, some electrolyte degradation compounds such as gaseous species may be generated at the positive electrode during charge and migrate to the negative electrode where they react to form Li_2O at the outermost surface of the SEI. When VC is used, the formation of Li_2O is nearly suppressed indicating that the possible reaction pathway proposed to form Li_2O would be almost eliminated by VC. Therefore, VC should have a major effect on the electrolyte/NMC interface in addition to the suppression of some parasitic reactions at the electrolyte/graphite interface which

would be expected from the improved electrochemical performances (Figures 5 and 6). Furthermore, for VC, the O1s core spectra present an important feature at 534.5 eV which is an uncommon very high binding energy. This latter is assigned to the formation of an oligomer of VC (Oligo-VC) in agreement with the previous studies of Ota *et al.*[18] and Ouatani *et al.*[20].

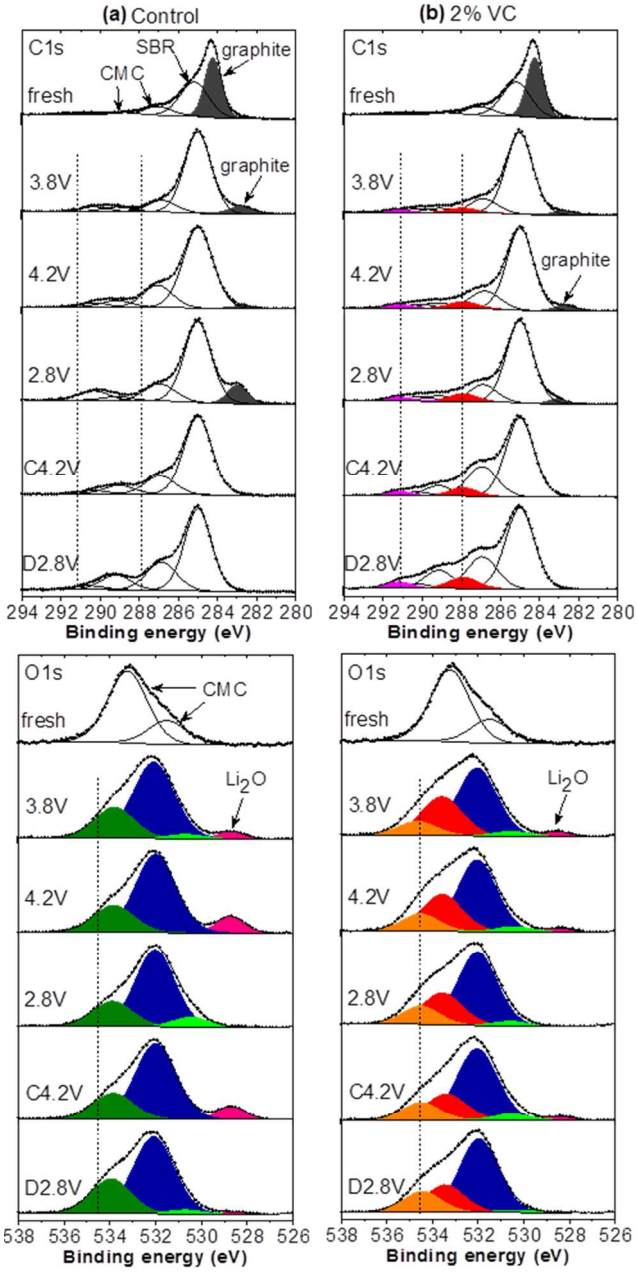

Figure 7. C1s and O1s XPS core spectra for graphite electrodes at 40°C (a) with 1M $LiPF_6$ EC:EMC electrolyte referred to as control and (b) with the addition of 2% VC.

Positive $LiNi_{1/3}Mn_{1/3}Co_{1/3}O_2$ electrodes.

The C1s core spectra of NMC electrodes are dominated by the PVdF and carbon black contributions due to the covering effect of the active material by the PVdF binder and to the high surface area of the carbon. This phenomenon leads to a very difficult interpretation of these C1s core spectra as often reported in the literature[20,21,54]. For this reason, Figure 8a shows only the typical C1s core spectra of NMC electrodes for control (black) and 2% VC (green) electrolytes as well as the difference spectrum (bottom) to allow a more thorough comparison. For both control and VC, five C1s peaks are observed as for the fresh electrode (not shown). The first one at 284.5 eV is attributed to C=C from the carbon black while the peaks at 286.2 and 290.8 eV arise from CH_2- and CF_2-like carbons of the PVdF binder respectively. The peaks at 287 and 288.9 eV could be due to CO_x-like species from the degradation of carbonate solvents. However, as they were also observed in the fresh electrode with similar intensity (not shown), the exact interpretation is rather difficult. The difference spectrum presented in Figure 8a (corresponding to the green area – shown at the bottom) allows one to highlight an important difference between 2% VC and control electrolytes. It reveals that when VC is used, two additional components are present at 288.1 and 290.9 eV with a 2:1 ratio. These peaks are close to the peak positions previously observed on the graphite electrodes for the 2% VC electrolyte. More importantly, this important feature is observed in the difference spectra whatever the state of charge is during formation and after cycling. Similarly, these two peaks at 288.1 and 290.9 eV are also observed

when VC is used in combination with TMS or DTD as discussed latter. Therefore, these two peaks are assigned with some confidence to the formation of Oligo-VC at the surface of the NMC electrodes. This result is in agreement to the peak position and interpretation described by Ouatani *et al*. for $LiCoO_2$/graphite cells formed at 3 V in pure VC[20].

Figure 8b shows the O1s spectra of the NMC electrodes for control and 2% VC electrolytes after formation at 4.2 V. The O1s spectrum of the fresh electrode shows a peak at 529.6 eV characteristic of O^{2-} anions of the lattice oxygen from the $LiNi_{1/3}Mn_{1/3}Co_{1/3}O_2$ active material and a peak at 531.7 eV assigned to oxygen atoms near defects at the NMC surface. For both control and VC electrolytes, after formation at 4.2 V (Figure 8b), a decrease of the O1s peak from NMC at 529.6 eV is observed and is attributed to the formation of a SEI film at the positive electrode/electrolyte interface which covers the active material, reducing the intensity of the 529.6 eV peak. In the case of VC, this decrease is more pronounced, indicating a thicker SEI as similarly observed in a previous study on $LiCoO_2$[20]. After cycling (Figure 8c) the intensity of the NMC peak is significantly lower for control electrolyte compared to VC electrolyte. This result suggests that during formation, VC-containing electrolyte produces a more stable and/or more protective SEI which results after cycling in a thinner SEI compared to control electrolyte. Therefore, VC greatly contributes to the reduction of parasitic reactions at the electrolyte/NMC interface which can explain the better electrochemical performance observed (Figures 5c, 5d and 6).

For control electrolyte, two peaks appear at 531.7 eV and 533.5 eV with an increasing intensity between formation and cycling (Figures 8b and c). These components may be attributed to CO_2-

like oxygen from carbonate compounds like LEDC and/or other $ROCO_2Li$ species and C-O linkages from $ROCO_2Li$ and/or polyethers[43,45,46] respectively. In the case of VC-containing electrolyte, the peak at 533.5 eV is replaced by two new components at 533.1 and 534.2 eV. It is suggested that the peak at 533.1 eV results from a shift of the peak at 533.5 eV for control electrolyte due to a specific reactivity of VC. Similarly to the graphite electrode (Figure 7), the peak at a very high binding energy of 534.2 eV is assigned to the formation of Oligo-VC[20].

These results highlight that the formation of Oligo-VC occurs at both the surface of graphite and NMC electrodes and is probably the origin of the more stable and/or more protective SEI films when VC is used compared to control electrolyte with no additive. VC therefore reduces parasitic reactions which results in lower CIE, lower charge end point capacity slippage and lower voltage drop during storage (Figure 5) and consequently in higher capacity retention (Figure 6).

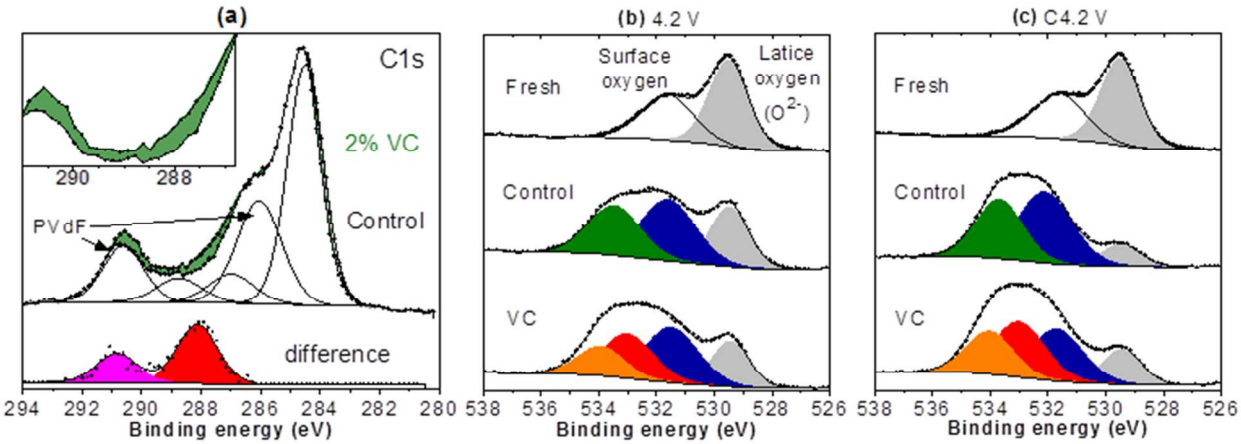

Figure 8. (a) Typical C1s XPS core spectra of $LiNi_{1/3}Mn_{1/3}Co_{1/3}O_2$ electrodes at 40°C for control (black) and 2% VC (green) electrolytes and the corresponding difference spectrum (bottom). O1s XPS core spectra of $LiNi_{1/3}Mn_{1/3}Co_{1/3}O_2$ electrodes at 40°C for control and 2% VC electrolytes at 4.2 V (b) during formation and (c) after cycling.

3.3 XPS analysis for TMS-based electrolytes

Graphite negative electrodes.

Figure 9 shows the C1s and O1s core spectra of the graphite electrodes from cells with 2% TMS or 2% VC + 2% TMS electrolytes compared to control and 2% VC electrolytes taken during formation and after 24 cycles. As the first charge occurs, both electrolytes containing TMS show a decrease in the graphite peak at 284.3 eV arising from the formation of SEI films at the surface of the graphite electrodes. After discharge to 2.8 V, 2% TMS (Figure 9c) shows an increase of the graphite component while no change is observed for 2% VC + 2% TMS (Figure 9d). After cycling, for both 2% TMS and 2% VC + 2% TMS electrolytes, the SEI thickness has increased to become higher than 5-10 nm as the graphite peak is not visible. These features of the graphite peak for 2% TMS and 2% VC + 2% TMS electrolytes follow the exact evolution observed for control and 2% VC electrolytes respectively (see Figure 7). Similarly, the peaks at 287 and 288.6 eV corresponding to the CO_x carbon environments from carbonaceous products show no apparent difference between 2% TMS and control as well as between 2% VC + 2% TMS and 2% VC. When VC is used in addition to TMS (Figure 9d), the two peaks at 287.9 and 291.3 eV are attributed to Oligo-VC as they have the exact same positions, 2:1 ratio and intensities as when VC is used alone. These results suggest that TMS has no significant effect on the SEI of graphite electrodes.

This result is supported by the evolution of the corresponding O1s spectra for TMS used singly or in combination with VC. Apart from a slightly lower contribution of the C-O peak at 533.5-533.8 eV (arising from $ROCO_2Li$ and/or polyether[45,46]) during formation for 2% TMS compared

to control and a slightly higher intensity after cycling for 2% VC + 2% TMS compared to 2% VC, no other apparent difference can be evidenced. The peak at 532 eV, characteristic of CO_2-like oxygen from LEDC[43] and/or other ($ROCO_2Li$) species[45,46] as well as the components at 530.7 and 528.6 eV assigned to ROLi and Li_2O respectively[50] are the same for TMS-containing electrolytes and the corresponding TMS-free electrolytes. For instance, when VC is added to TMS (Figure 9d), the formation of Li_2O is almost eliminated just as observed for 2% VC electrolyte (Figure 9b). The O1s peak at a high binding energy of 534.5 eV previously attributed to Oligo-VC when VC is used alone (Figure 7) is still observed with similar intensity when TMS is added (Figure 9d). Therefore, in agreement with the observation of the C1s core spectra, TMS has nearly no impact on the chemical nature and the amount of the SEI species arising from the degradation of carbonate solvents at the surface of graphite electrodes both during the formation and cycling of NMC/graphite pouch cells.

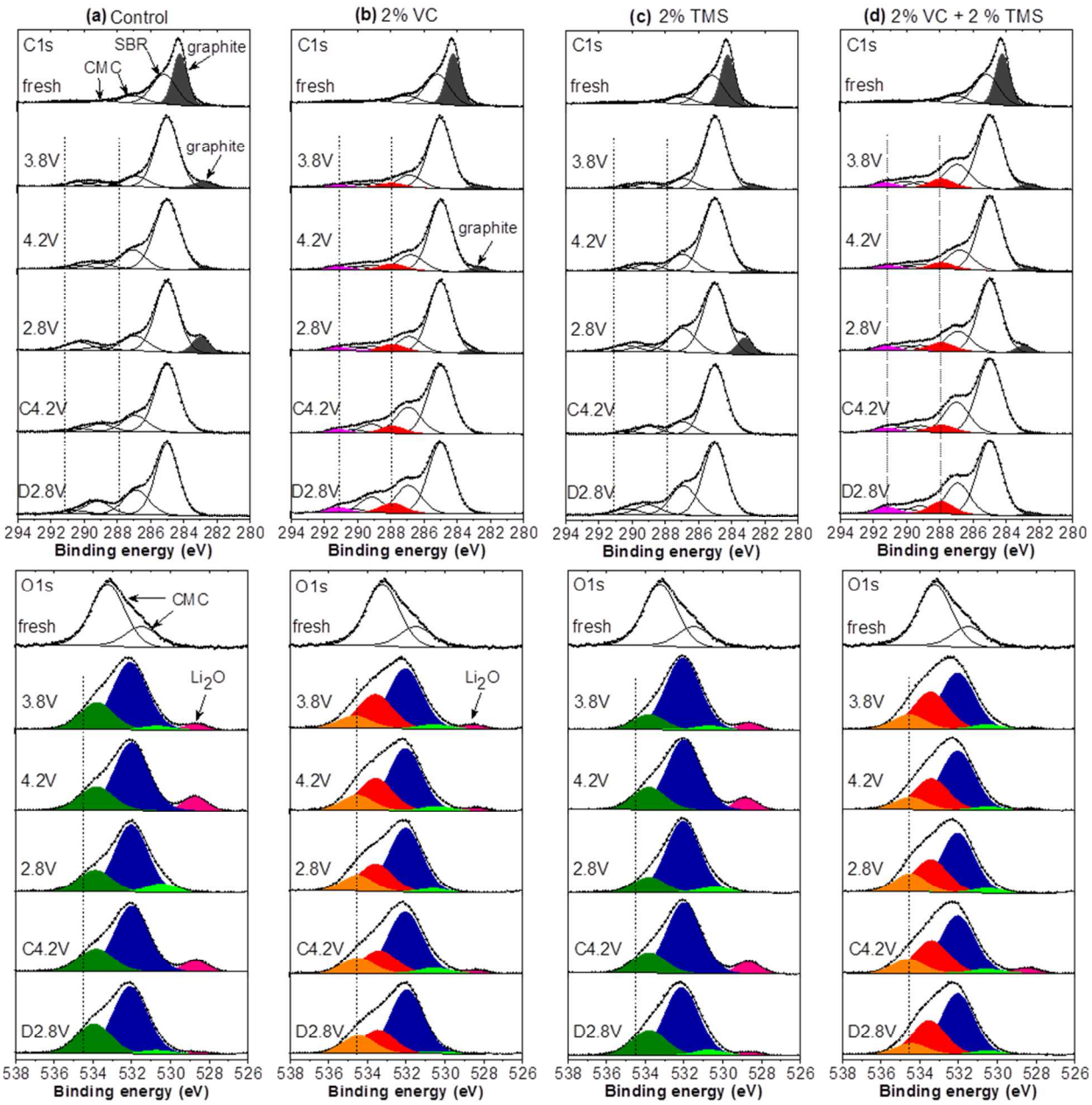

Figure 9. C1s and O1s XPS core spectra for graphite electrodes at 40°C with (a) control, (b) 2% VC, (c) 2% TMS and (d) 2% VC + 2 % TMS electrolytes.

Positive $LiNi_{1/3}Mn_{1/3}Co_{1/3}O_2$ electrodes.

Figure 10 shows the O1s core spectra of the NMC electrodes from cells that contained 2% TMS or 2% VC + 2% TMS electrolytes compared to control and 2% VC electrolytes. During the first charge, both TMS-containing electrolytes show a decrease of the NMC peak at 529.6 eV due to the formation of SEI films at the positive electrode/electrolyte interfaces which cover the NMC surface. For the TMS-containing electrolytes (Figures 10c and d), this peak during formation and cycling is identical to those of the corresponding TMS-free electrolytes (Figures 10a and b) which indicates similar SEI thicknesses. Similarly, the contribution of the CO_2 (from LEDC and/or other $ROCO_2Li$ species) and C-O (from $ROCO_2Li$ and/or polyethers) environments at 531.7 and 533.1-533.5 eV, respectively, show no apparent difference between TMS-containing and the corresponding TMS-free electrolytes. When VC is used in addition to TMS, the peak observed for VC as single additive at a very high binding energy of 534.2 eV appears and is assigned to the formation of Oligo-VC[20]. Additionally, as mentioned earlier, the difference C1s spectra between 2% VC + 2% TMS and 2% TMS electrolytes shows two additional peaks at 288.1 and 290.9 eV with a 2:1 ratio when VC is added to TMS (not shown) and the peaks are assigned to Oligo-VC at the NMC electrode surface[20]. Therefore, when VC is used both alone and in combination to TMS, it contributes identically to the SEI films through the formation of Oligo-VC at the surface of both graphite and NMC electrodes.

Based on the XPS results for TMS discussed above, it is therefore consistent that 2% VC and 2% VC + 2% TMS electrolytes show similar electrochemical performances (Figure 5 and 6). Based on the C1s and O1s spectra for the graphite electrodes (Figure 9) and O1s spectra for NMC electrodes (Figure 10), TMS does not affect the chemical nature or amounts of the C- and O-based species of the SEI on both electrodes of NMC/graphite pouch cells. At this point, the moderate performance gain (Figure 5) associated with a slightly lower capacity fade (Figure 6)

observed when TMS is used singly compared to control electrolyte could be due to either different F- and P-based species or the formation of sulfur compounds at the surface of both graphite and NMC electrodes. This point is discussed later.

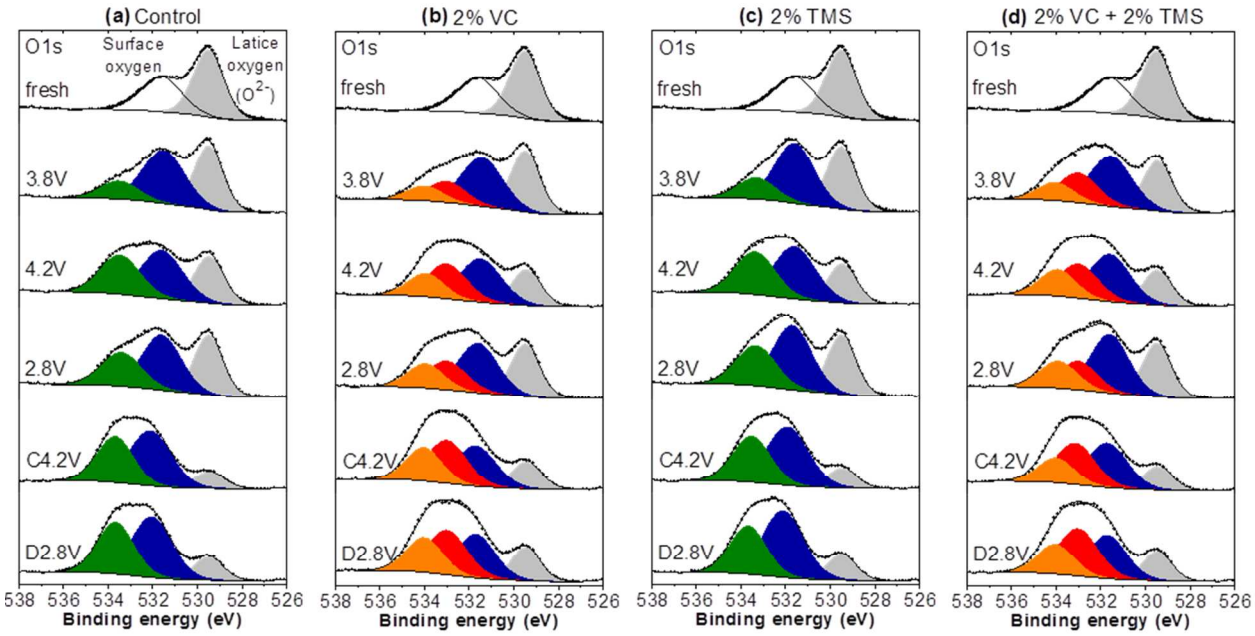

Figure 10. O1s XPS core spectra for $LiNi_{1/3}Mn_{1/3}Co_{1/3}$ electrodes at 40°C with (a) control, (b) 2% VC, (c) 2% TMS and (d) 2% VC + 2 % TMS electrolytes.

3.3 XPS analysis for DTD-based electrolytes

Graphite negative electrodes

Figure 11 compares the C1s and O1s core spectra of the graphite electrodes of NMC/graphite pouch cells at various SOC and cycle number for electrolytes with 2% DTD or 2% VC + 2% DTD to results for electrodes tested with control or 2% VC electrolytes, respectively. During formation, both DTD-containing electrolytes (Figures 11c and d) show a similar evolution of the

graphite peak at 284.3 eV compared to 2% VC electrolyte. This graphite component decreases during the first charge which results from the formation of SEI films on the graphite electrode surface. After the subsequent discharge no significant further change of this peak is observed. This result suggests that DTD, like VC, produces a more stable (at least as thickness is concerned) SEI film on the graphite electrodes compared to control electrolyte. After cycling, for both DTD-containing electrolytes (Figures 11c and d), the graphite peak at 284.3 eV remains slightly visible compared to control and VC electrolytes which suggests a lower SEI thickness on graphite electrodes when DTD is used. Additionally, when DTD is used alone and in combination with VC (Figures 11c and d), different ratios of oxygenated species are observed compared to control and VC electrolytes probably due to a different reactivity of the carbonate solvents that occurs after that DTD has been preferentially reduced at the surface of the graphite electrode (Figure 3). The peak of CO-like carbon at 287 eV for DTD-containing electrolytes is almost identical to that of control and 2% VC electrolytes, but the peak of CO_2-like carbon at 288.6 eV clearly exhibits a lower intensity. Similarly, the O1s spectra of graphite electrodes tested in DTD-containing electrolytes show a lower contribution of the C-O peak at 533.5-533.8 eV (Figures 11c and d) compared to control and VC electrolytes.

It is difficult at this point to determine which O-based species are formed in the presence of DTD although Sano *et al*.[29] have reported that DTD might form a polyethylene oxide (PEO) polymer in PC-containing electrolytes. It is clear, however, that DTD significantly changes the chemical nature of the SEI. For instance, at 2.8V after cycling, the amount of carbon and oxygen at the surface of the graphite electrode tested with DTD accounts for 42 at. % and 29 at. % of the SEI according to XPS, respectively, compared to 36 at. % and 22 at. %, respectively, for control electrolyte. It is possible that this can be explained by a lower reactivity of the $LiPF_6$ salt when

DTD is used as will be discussed later. When DTD is used in combination with VC, the decrease of the O1s component at 533.8 eV is less apparent, especially after cycling, suggesting a less significant effect of DTD when VC is also present. Similarly, the use of DTD helps to reduce the formation of Li_2O (O1s peak at 528.6 eV) with a more pronounced effect when DTD is used alone (Figure 11c). Graphite electrodes tested in cells with 2% DTD electrolyte form a larger amount of ROLi species (O1s peak at 530.7 eV) than control and VC electrolytes. When VC is used with DTD, both C1s (at 287.9 and 291.3 eV with a 2:1 ratio) and O1s (at 534.5 eV) features of Oligo-VC[20] appear with moderate intensities compared to when VC is used alone. These results show that for graphite electrodes, 2% VC + 2% DTD-containing electrolyte yields almost the same SEI features of DTD used alone plus half the SEI features of VC used alone as it could be expected from the dQ/dV and GC-MS analysis (Figures 3 and 4).

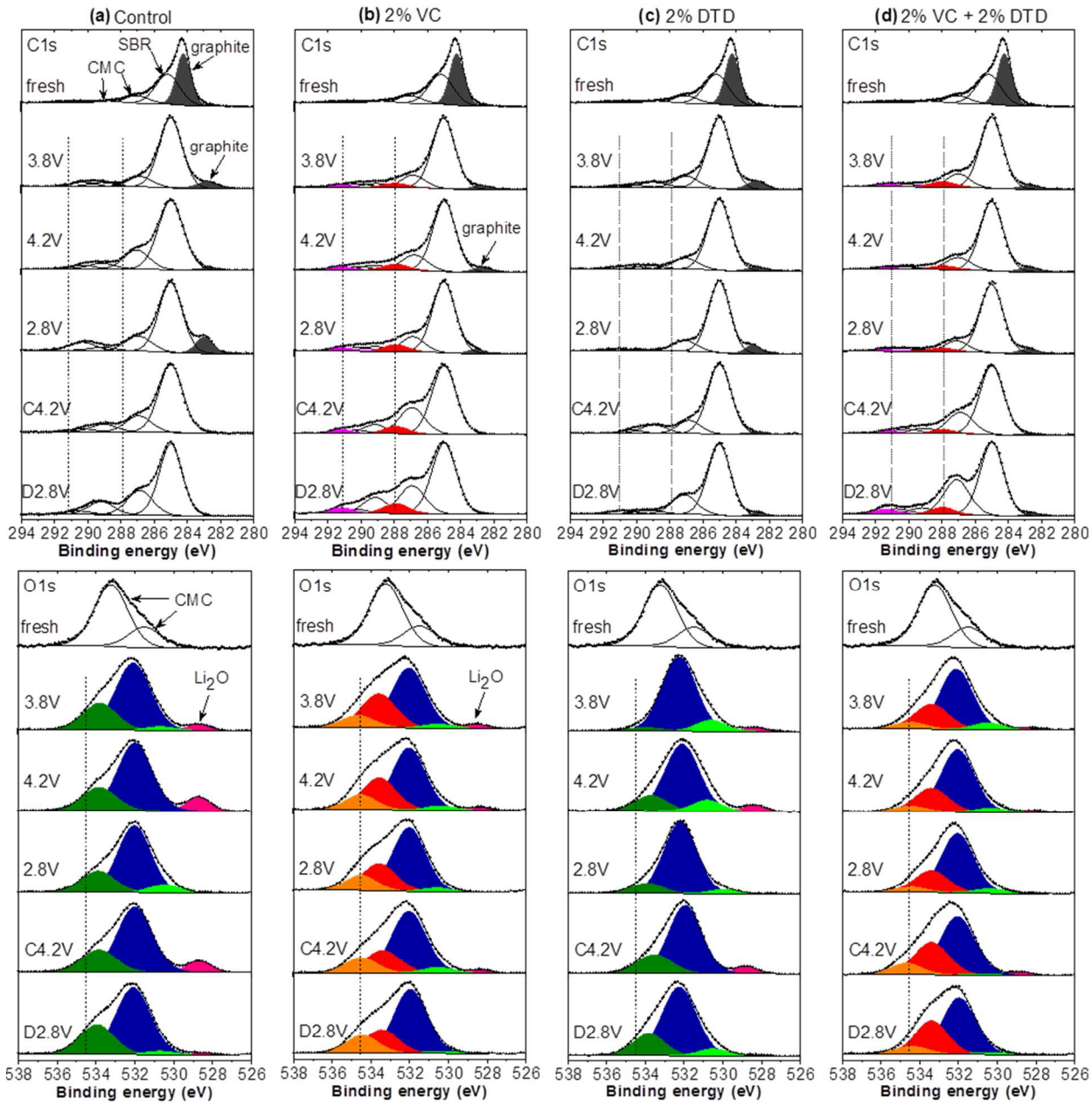

Figure 11. C1s and O1s XPS core spectra for graphite electrodes at 40°C with (a) control, (b) 2% VC, (c) 2% DTD and (d) 2% VC + 2 % DTD electrolytes.

Positive $LiNi_{1/3}Mn_{1/3}Co_{1/3}O_2$ electrodes.

Figure 12 compares the O1s core spectra of the NMC electrodes taken from cells tested with 2% DTD or 2% VC + 2% DTD electrolytes to those from cells tested with control or 2% VC electrolytes, respectively. Both DTD-containing electrolytes (Figures 12c and d) show a similar evolution of the NMC peak at 529.6 eV during formation compared to 2% VC electrolyte. The NMC component at 529.6 eV decreases during the first charge as SEI films are formed at the NMC electrode surface then this peak slightly increases after discharge due to dissolution/consumption of SEI species. After cycling, in the case of 2% DTD electrolyte (Figure 12c), the contribution of the NMC peak at 529.6 eV is higher compared to control and 2% VC electrolytes which point out a thinner SEI on NMC electrodes when DTD is used alone. These results suggest that DTD, like VC, produces a more stable and/or more protective SEI on the NMC electrodes than control electrolyte.

As previously observed for graphite electrodes (Figure 11), the use of DTD leads to different ratios of O-containing species at the surface of the NMC electrodes compared to control and VC electrolytes. For instance, the C-O peak at 533.5-533.8 eV (Figures 12c and d) shows lower contribution during formation and after cycling compared to control and VC electrolytes. When VC is used with DTD, the O1s component characteristic of Oligo-VC at 534.2 eV[20] appears with moderate intensity. The difference C1s spectra between 2% VC + 2% DTD and 2% DTD electrolytes reveals the corresponding two C1s peaks of Oligo-VC at 288.1 and 290.9 eV (not shown). Similarly to the graphite electrodes, the SEI film formed with 2% VC + 2% DTD electrolyte at the surface of the NMC electrode shows almost the same characteristics as DTD used alone plus half the feature of VC used alone.

Therefore, DTD has a significant impact on the chemical nature of the C- and O-containing species of the SEI on both electrodes of NMC/graphite pouch cells. The chemical nature of the SEI is found to be identical on both the graphite and the NMC electrodes which highlight a similar reactivity of DTD at both electrode surfaces. The effect of DTD on the further degradation of the carbonate solvents therefore improves the CIE, charge end point capacity slippage (Figure 5) and the resulting capacity retention (Figure 6) in such a way that competes with VC-containing electrolyte.

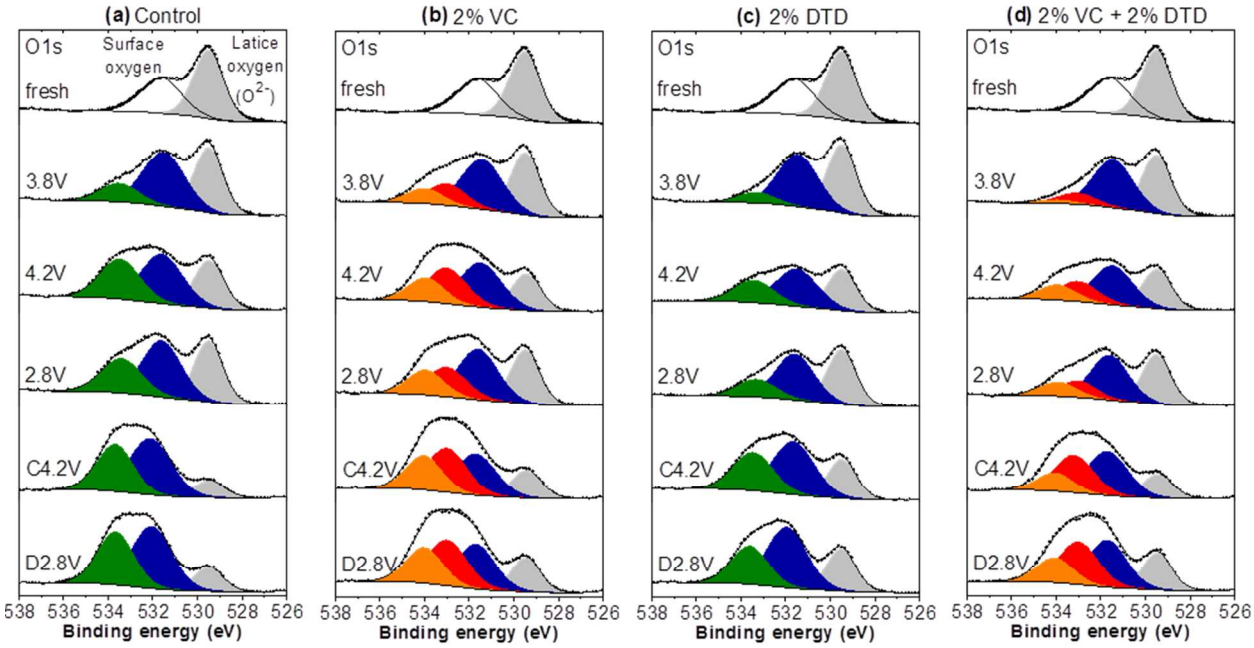

Figure 12. O1s XPS core spectra for $LiNi_{1/3}Mn_{1/3}Co_{1/3}$ electrodes at 40°C with (a) control, (b) 2% VC, (c) 2% DTD and (d) 2% VC + 2 % DTD electrolytes.

3.3 Further studies on F-, P- and S-based species

To complete the XPS study of the SEI on both graphite and $LiNi_{1/3}Mn_{1/3}Co_{1/3}O_2$ electrodes, this section presents the analysis of the F1s, P2p and S2p core spectra. Figure 13 shows the typical F1s and P2p XPS core spectra for graphite and $LiNi_{1/3}Mn_{1/3}Co_{1/3}O_2$ electrodes. Both negative

and positive electrodes show two F1s components. The first peak at 685.3-685.6 eV corresponds to LiF[46,55] that results from the degradation of the $LiPF_6$ salt[56,57]. For graphite electrodes, the second peak at 687.6 eV is assigned to Li_xPF_y [58] and to fluorophosphates ($Li_xPO_yF_z$)[56,57] that arise from the degradation of the $LiPF_6$ salt[59,60] as well as to possible remaining $LiPF_6$ salt despite the washing procedure of the electrodes (see experimental section). In the case of NMC electrodes, the second peak at 687.8 eV in Figure 12 is attributed mostly to the PVdF binder in addition to some $Li_xPO_yF_z$ species.

The P2p spectra in Figure 13 show three and two components (e.g. doublets that include $2p_{3/2}$ and $2p_{1/2}$ core peaks separated by 0.9 eV) for the graphite and NMC electrodes, respectively. The first peak at 133.6-133.8 eV is assigned to phosphates (P_xO_y) while the second at 135.2-135.6 eV corresponds to fluorophosphates ($Li_xPO_yF_z$)[20,55]. For graphite electrodes, the third peak at 137.3 eV is attributed Li_xPF_y [58], fluorophosphates ($Li_xPO_yF_z$)[20,55] as well as possible remaining $LiPF_6$ salt. These results suggest that Li_xPF_y/$LiPF_6$ are only present on the negative graphite electrodes as similarly observed by Bouayad *et al*. for $LiNi_{0.5}Mn_{0.5}O_4$/$Li_4Ti_5O_{12}$ coin cells[55].

At this point, no clear evolution of the Li_xPF_y/$LiPF_6$ content at the surface of the graphite electrodes can be observed whatever the electrolyte is. The atomic percentage (at. %) of LiF is reported in Table 1 for both graphite and $LiNi_{1/3}Mn_{1/3}Co_{1/3}O_2$ electrodes. During formation, the amount of LiF increases during charge while after discharge it decreases suggesting that LiF is possibly consumed or buried during discharge. More importantly, LiF appears to be present throughout the entire thickness of the SEI. Indeed, if LiF was only deposited close to the graphite material surface, it would be unlikely that its content could be reduced during discharge while the SEI thickness decreases. For graphite electrodes, this phenomenon is still observed after cycling indicating that LiF continues to be formed and consumed during cycling. This

observation suggests that LiF is more likely formed via an electrochemical reduction of PF_6^- anion rather than via an impurity from hydrolysis.

After cycling, the LiF content for NMC electrodes slightly increases during discharge while the SEI thickness was found to slightly decrease. LiF is therefore preferentially formed close to the NMC active material surface during formation and the cycling does not lead to further formation/consumption of LiF on the NMC electrode surface. More generally, the LiF content is two to five times higher at the surface of graphite electrodes (Table 1) which suggests a lower reactivity of the $LiPF_6$ salt at the surface of the NMC active material. This is supported by the higher amount of phosphates (P_xO_y) and fluorophosphates ($Li_xPO_yF_z$) species measured at the surface of graphite electrodes (See Tables S1 and S2) that arise from the degradation of the $LiPF_6$ salt[56,57,59,60]. For graphite electrodes, the amount of P_xO_y is higher than the amount of $Li_xPO_yF_z$ while for positive electrodes, the opposite trend is observed (See Tables S1 and S2). This result suggests a different reactivity of the $LiPF_6$ salt at the surface of graphite and NMC electrodes.

When TMS is used alone, the evolution of the LiF content (Table 1) as well as those of P_xO_y and $Li_xPO_yF_z$ (Tables S1 and S2) are very similar to those observed for control electrolyte. This result means that TMS used alone leads to a similar SEI composition and evolution compared to control electrolyte as stated before. 2% TMS electrolyte differs therefore from control electrolyte only for the presence of a small amount of sulfur-based species on both graphite and NMC electrodes as discussed below. Surprisingly, it appears that VC used either alone or in combination with TMS yields a similar amount of LiF (Table 1), P_xO_y and $Li_xPO_yF_z$ (Tables S1 and S2) compared to control electrolyte with few exceptions. VC has therefore no significant impact on the formation of F- and P-containing species. On the other hand, DTD greatly reduces

the formation of LiF and the corresponding P-containing species that result from the degradation of the $LiPF_6$ salt. When VC is added in combination with DTD, the amount of the $LiPF_6$ degradation products are further decreased indicating a possible cooperative effect between DTD and VC. DTD therefore significantly changes the chemical nature of the SEI film by decreasing the proportion of inorganic compounds in the SEI composition at the surface of both graphite and NMC electrodes.

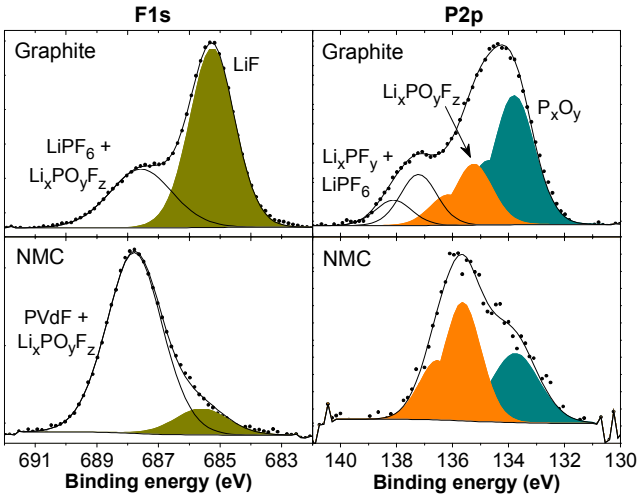

Figure 13. Typical F1s and P2p XPS core spectra of graphite and $LiNi_{1/3}Mn_{1/3}Co_{1/3}O_2$ electrodes at 40°C for the different electrolytes studied. The example given here corresponds to cell formed with control electrolyte at 4.2 V.

Table 1. Atomic percentage (at. %) of LiF measured at the surface of graphite and NMC electrodes as function of the voltage of the cell during formation and after cycling.

Sample	Graphite					$LiNi_{1/3}Mn_{1/3}Co_{1/3}O_2$				
	3.8V	4.2V	2.8V	C4.2V	D2.8V	3.8V	4.2V	2.8V	C4.2V	D2.8V
Control	15.4	16.3	12.3	11.6	9.2	1.3	2.5	2.0	2.6	2.8

2% VC	5.4	6.0	5.4	12.8	12. 3	2.2	4.8	1.9	2.4	3.5
2% TMS	12.6	12.2	7.8	11.9	6.1	1.2	3.0	1.8	2.6	2.5
2% VC + 2% TMS	11.34	13.2	2.9	8.5	6.2	5.5	5.1	2.4	2.2	2.4
2% DTD	3.2	7.9	3.8	6.0	2.5	1.1	2.5	2.0	2.6	2.9
2% VC + 2% DTD	2.0	4.7	3.5	4.1	1.2	1.6	2.4	2.1	2.3	2.4

Figure 14a shows the typical S2p XPS core spectra for graphite and $LiNi_{1/3}Mn_{1/3}Co_{1/3}O_2$ electrodes. One peak is observed at 169.2 and 168.7 eV for the graphite and NMC electrodes respectively. Note that the S2p core spectra for the reference TMS and DTD additives show only one peak at 169 ± 0.1 eV (Figure S2). Considering the small binding energy difference of the S2p component observed between the negative and the positive electrodes, it is more likely that this peak arises from similar species. The S2p peak is therefore attributed to sulfate (RSO_4) compounds such as Li_2SO_4 and/or sulfite species (RSO_3) such as $ROSO_2Li$ that have been reported in the range 168.5-169.5 eV[61]. Concerning the S content (Figure 14b), TMS forms globally much less sulfur compounds than DTD during formation as it could have been expected from the GC-MS analysis (Figure 4). This tendency continues with cycling which denotes a clearly higher and different reactivity of DTD. The amount of sulfur species in the SEI composition is almost two times higher at the surface of the graphite electrodes. Note also that the proportion of the S-containing species in the SEI composition remains almost constant after formation at 3.8 V.

As a summary, when TMS is used either alone or in combination with VC, the SEI composition (*i.e.* C-, O-, F- and P-based species) and its evolution are similar to those of the respective TMS-free electrolytes as it was partially suggested from the dQ/dV and GC-MS analysis (see Figures 3 and 4). TMS forms, however, a small amount of S-containing species at the surface of both electrodes that may induce the moderate electrochemical performance gain observed when TMS

is used alone (Figure 5 and 6). On the other hand, DTD shows a higher and more beneficial reactivity than TMS although these two additives are homologous molecules that differ only by one carbon atom in their carbon-ring (Figure 1). At this point, it may be explained by the electrochemical reaction of DTD that occurs before the reduction of EC which is not the case for TMS (Figure 3). Apparently, DTD induces a different reactivity of the carbonate solvents as well as the $LiPF_6$ salt. The greatly different chemical nature and composition of the SEI films formed at the surface of both graphite and NMC electrodes by DTD compared to control and VC electrolytes appears therefore to be at the origin of the enhancement of the electrochemical performances with DTD (Figure 5 and 6). Finally, when VC is used alone or in combination with TMS, the formation of Oligo-VC at the surface of both electrodes leads to the higher electrochemical performance compared to control. When VC is added to DTD, however, both additives contribute to the improvement of the electrochemical performance.

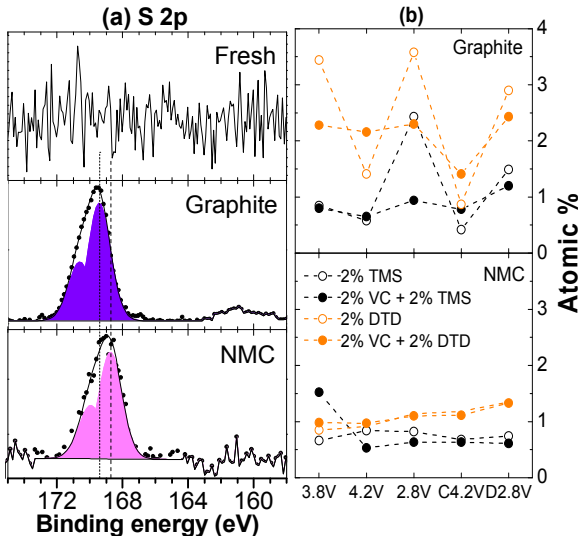

Figure 14. (a) Typical S2p XPS core spectra for graphite or $LiNi_{1/3}Mn_{1/3}Co_{1/3}O_2$ electrodes cycled at 40°C for TMS- and DTD-based electrolytes and (b) evolution of the S content at the

surface of graphite and $LiNi_{1/3}Mn_{1/3}Co_{1/3}O_2$ electrodes at 40°C for TMS- and DTD-containing electrolytes as determined from XPS quantification.

Conclusion

The role of two homologous cyclic sulfate additives, TMS and DTD, used alone or in combination with VC, on the lifetime of NMC/graphite pouch cells has been thoroughly examined. GC-MS has been used as a powerful tool to support the interpretation of the dQ/dV plots recorded during the early stages of the formation cycle. Ultra high precision coulometry and storage experiments have been performed to highlight the differences of CIE, charge end point capacity slippage and voltage drop during storage between the different electrolyte compositions. Thorough XPS analysis of the SEI films formed at both negative and positive electrodes during formation and after cycling has then been conducted to probe the role of the additives used and has been correlated to the electrochemical performances.

As the two sulfate additives have been used alone or in combination with VC, the first part of the XPS studies has been devoted to the characterization of the SEI for the control and VC cells. It has been shown that VC forms a polymer (*i.e.* Oligo-VC) at the surface of both graphite and NMC electrodes during formation which results in more stable (at least as far as thickness goes) SEI films. The apparent reduction of parasitic reactions when VC is used explains the lower CIE, charge end point capacity slippage and voltage drop during storage observed and the resulting higher capacity retention compared to control electrolyte.

For TMS-containing electrolytes, strictly similar chemical SEI compositions and evolutions were observed compared to the the respective TMS-free electrolytes in good agreement with the

proposals made initially from the dQ/dV and GC-MS analysis. The relatively moderate electrochemial performance gain observed when TMS was used alone may be caused by the formation of a small amount of sulfate compounds at the surface of both electrodes. For 2% VC + 2% TMS, the higher cell lifetime observed was due to the addition of VC and the resulting formation of Oligo-VC.

The use of the homologous DTD additive lead to electrochemical performances that can compete with VC more likely due to a preferential reduction potential compared to TMS. This higher reactivity of DTD might explain the two times higher sulfur content in both SEI compositions measured by XPS. It has been suggested that DTD induces a different reactivity of both the carbonate solvents and the $LiPF_6$ salt compared to control and VC electrolytes. The SEI films formed by DTD had a much lower fraction of inorganic compounds arising from the degradation of the $LiPF_6$ salt that results in a higher fraction of organic species. When VC was added to DTD, both additives contributed to the formation of the SEI films with an apparent contribution of each additive similar to the initial reactivity observed from the dQ/dV and GC-MS analysis.

Finally, the results of this study demonstrate that thorough analysis of the SEI films formed by electrolyte additives is highly relevant and reliable when correlated to precise electrochemical performance data and suggests that a better understanding of the exact role of such additives on cell lifetime is important for future improvements.

ASSOCIATED CONTENT

Supporting Information. Atomic percentage (at. %) of of phosphates and fluorophosphates measured at the surface of graphite and $LiNi_{1/3}Mn_{1/3}Co_{1/3}O_2$ electrodes. S2p XPS core spectra for TMS and DTD additives.

AUTHOR INFORMATION

Corresponding Author

*E-mail: jeff.dahn@dal.ca

ACKNOWLEDGMENT

The authors acknowledge financial support of this work by 3M Canada and NSERC under the auspices of the Industrial Chairs Program. Support from NSERC Automotive Partnership is also gratefully acknowledged. R.Petibon and K.J. Nelson acknowledge NSERC for scholarship support.

TOC graphic:

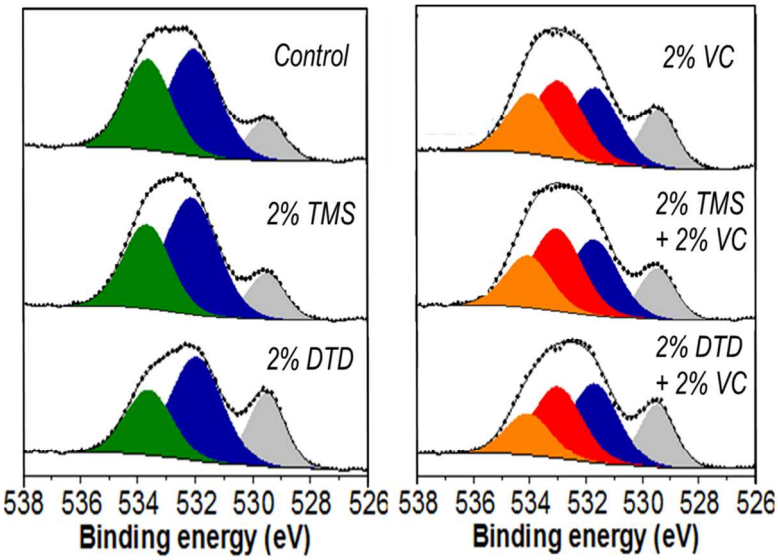
Control
2% TMS
2% DTD
2% VC
2% TMS
+ 2% VC
2% DTD
+ 2% VC
538 536 534 532 530 528 526
Binding energy (eV)
538 536 534 532 530 528 526
Binding energy (eV)

REFERENCES

(1) Zhang, S. S. A Review on Electrolyte Additives for Lithium-ion Batteries. *J. Power Sources*, **2006**, *162*, 1379-1394.
(2) Xu, K. Nonaqueous Liquid Electrolytes for Lithium-Based Rechargeable Batteries**.** *Chem. Rev.*, **2004**, *104*, 4303-4418.
(3) Peled, E. The Electrochemical Behavior of Alkali and Alkaline Earth Metals in Nonaqueous Battery Systems - The Solid Electrolyte Interphase Model. *J. Electrochem. Soc*., **1979**, *126*, 2047-2051.
(4) Simon, B.; Boeuve, J.-P. Rechargeable Lithium Electrochemical cell. US Patent, **1997**, 5,626,981.
(5) Zhang, X.; Kostecki, R.; Richardson, T.J.; Pugh, J.K.; Ross Jr, P. N. Electrochemical and Infrared Studies of the Reduction of Organic Carbonates. *J. Electrochem. Soc.*, **2001**, *148*, A1341-A1345.
(6) Aurbach, D.; Gamolsky, K.; Markovsky, B.; Gofer, Y.; Schmidt, M.; Heider, U. On the Use of Vinylene Carbonate (VC) as an Additive to Electrolyte Solutions for Li-Ion Batteries. *Electrochim. Acta*, **2002**, *47*, 1423-1439.
(7) Mogi, R.; Inaba, M.; Jeong, S.-K.; Iriyama, Y.; Abe T.; Ogumi, Z. Effects of Some Organic Additives on Lithium Deposition in Propylene Carbonate**.** *J. Electrochem. Soc.*, **2002**, *149*, A1578-A1583.
(8) Ota, H.; Shima, K.; Ue, M.; Yamaki, J.-I. Effect of Vinylene Carbonate as Additive to Electrolyte for Lithium Metal Anode. *Electrochim. Acta*, **2004**, *49*, 565-572.
(9) Contestabile, M.; Morselli, M.; Paraventi R.; Neat, R. J. A Comparative Study on the Effect of Electrolyte/Additives on the Performance of ICP383562 Li-Ion Polymer (Soft-Pack) Cells. *J. Power Sources*, **2003**, *119*, 943-947.
(10) Holzapfel M.; Jost, C.; Prodi-Schwab, A.; Krumeich, F.; Wursig, A.; Buqa H.; Novak, P. Stabilisation of Lithiated Graphite in an Electrolyte Based on Ionic Liquids: An Electrochemical and Scanning Electron Microscopy Study. *Carbon*, **2005**, *43*, 1488-1498.
(11) Sasaki, T.; Abe, T.; Iriyama, Y.; Inaba, M.; Ogumi, Z. Suppression of an Alkyl Dicarbonate Formation in Li-Ion Cells. *J. Electrochem. Soc*., **2005**, *152*, A2046-A2050.
(12) Shim, E.-G.; Nam, T.-H.; Kim, J.-G.; Kim, H.-S.; Moon, S.-I. Effects of Functional Electrolyte Additives for Li-Ion Batteries. *J. Power Sources*, **2007**, *172*, 901-907.
(13) Chen, L.; Wang, K.; Xie, X.; Xie, J. Effect of Vinylene Carbonate (VC) as Electrolyte Additive on Electrochemical Performance of Si Film Anode for Lithium Ion Batteries. *J. Power Sources*, **2007**, *174*, 538-543.
(14) Burns, J. C.; Jain, G.; Smith, A. J.; Eberman, K. W.; Scott, E.; Gardner, J. P.; Dahn, J. R. Evaluation of Effects of Additives in Wound Li-Ion Cells Through High Precision Coulometry. *J. Electrochem. Soc.*, **2011**, *158*, A255-A261.
(15) Sinha, N. N.; Smith, A. J.; Burns, J. C.; Jain, G.; Eberman, K. W.; Scott, E.; Gardner, J. P.; Dahn, J. R. The Use of Elevated Temperature Storage Experiments to Learn about Parasitic Reactions in Wound $LiCoO_2$/Graphite Cells. *J. Electrochem. Soc.*, **2011**, *158*, A1194-A1201.
(16) Jeon, J.; Yoon, S.; Park, T.; Cho, J.-J.; Kang, S.; Han, Y.-K.; Lee, H. Tuning glycolide as an SEI-forming additive for thermally robust Li-ion batteries. *J. Mater. Chem.*, **2012**, *22*, 21003-21008.
(17) Jung, H. M.; Park, S.-H.; Jeon, J.; Choi, Y.; Yoon, S.; Cho, J.-J.; Oh, S.; Kang, S.; Han, Y.-K.; Lee, H. Fluoropropane Sultone as an SEI-Forming Additive that Outperforms Vinylene Carbonate. *J. Mater. Chem. A*, **2013**, *1*, 11975-11981.
(18) Ota, H.; Sakata, Y.; Inoue, A.; Yamaguchi, S. Analysis of Vinylene Carbonate Derived SEI Layers on Graphite Anode. *J. Electrochem. Soc.*, **2004**, *151*, A1659-A1669.
(19) Wang, Y.; Nakamura, S.; Tasaki, K.; Balbuena, P. B. Theoretical Studies To Understand Surface Chemistry on Carbon Anodes for Lithium-Ion Batteries: How Does Vinylene Carbonate Play Its Role as an Electrolyte Additive? *J. Am. Chem. Soc*., **2002**, *124*, 4408-4421.

(20) El Ouatani, L.; Dedryvère, R.; Siret, C.; Biensan, P.; Reynaud, S.; Iratçabal, P.; Gonbeau, D. The Effect of Vinylene Carbonate Additive on Surface Film Formation on Both Electrodes in Li-Ion Batteries. *J. Electrochem. Soc.,* **2009**, *156*, A103-A113.
(21) El Ouatani, L.; Dedryvère, R.; Siret, C.; Biensan, P.; Gonbeau, D. Effect of Vinylene Carbonate Additive in Li-Ion Batteries: Comparison of $LiCoO_2$/C , $LiFePO_4$/C , and $LiCoO_2$/$Li_4Ti_5O_{12}$ Systems. *J. Electrochem. Soc.*, **2009**, *156*, A468-A477.
(22) Xu, M.; Li, W.; Lucht, B. L. Effect of Propane Sultone on Elevated Temperature Performance of Anode and Cathode Materials in Lithium-Ion Batteries. *J. Power Sources*, **2009**, *193*, 804-809.
(23) Zuo, X.; Fan, C.; Xiao, X.; Liu, J.; Nan, J. Methylene Methanedisulfonate as an Electrolyte Additive for Improving the Cycling Performance of $LiNi_{0.5}Co_{0.2}Mn_{0.3}O_2$/Graphite Batteries at 4.4 V Charge Cutoff Voltage. *ECS Electrochem. Letters*, **2012**, *1*, A50-A53.
(24) Li, B.; Xu, M.; Li, B.; Liu, Y.; Yang, L.; Li, W.; Hu, S. Properties of Solid Electrolyte Interphase Formed by Prop-1-ene-1,3-sultone on Graphite Anode of Li-Ion Batteries. *Electrochim. Acta*, **2013**, *105*, 1-6.
(25) Xia, J.; Sinha, N. N.; Chen, L. P.; Kim, G. Y.; Xiong, D. J.; Dahn, J. R. Study of Methylene Methanedisulfonate as an Additive for Li-Ion Cells. *J. Electrochem. Soc.*, **2014**, *161*, A84-A88.
(26) Xia, J.; Harlow, J. E.; Petibon, R.; Burns, J. C.; Chen, L. P.; Dahn, J. R. Comparative Study on Methylene Methyl Disulfonate (MMDS) and 1,3-Propane Sultone (PS) as Electrolyte Additives for Li-Ion Batterie. *J. Electrochem. Soc.*, **2014**, *161*, A547-A553.
(27) Xia, J.; Aiken, C. P.; Ma, L.; Kim, G. Y.; Burns, J. C.; Chen, L. P.; Dahn, J. R. Combinations of Ethylene Sulfite (ES) and Vinylene Carbonate (VC) as Electrolyte Additives in $Li(Ni_{1/3}Mn_{1/3}Co_{1/3})O_2$/Graphite Pouch Cells. *J. Electrochem. Soc.*, **2014**, *161*, A1149-A1157.
(28) Xia, J.; Ma, L.; Aiken, C. P.; Nelson, K. J.; Chen, L. P.; Dahn, J. R. Comparative Study on Prop-1-ene-1,3-sultone and Vinylene Carbonate as Electrolyte Additives for $Li(Ni_{1/3}Mn_{13}Co_{1/3})O_2$/Graphite Pouch Cells. *J. Electrochem. Soc.*, **2014**, *161*, A1634-A1641.
(29) Sano, A.; Maruyama, S. Decreasing the Initial Irreversible Capacity Loss by Addition of Cyclic Sulfate as Electrolyte Additives. *J. Power Sources*, **2009**, *192*, 714-718.
(30) Janssen, P.; Schmitz, R.; Müller, R.; Isken,P.; Lex-Balducci, A.; Schreiner, C.; Winter, M.; Cekić-Lasković, I.; Schmitz, R. 1,3,2-Dioxathiolane-2,2-dioxide as Film-Forming Agent for Propylene Carbonate Based Electrolytes for Lithium-Ion Batteries. *Electrochim. Acta*, **2014**, *125*, 101-106.
(31) Xia, J.; Sinha, N. N.; Chen, L. P.; Dahn, J. R. A Comparative Study of a Family of Sulfate Electrolyte Additives. *J. Electrochem. Soc*., **2014**, *161*, A264-A174.
(32) Smith, A. J.; Burns, J. C.; Trussler, S.; Dahn, J. R. Precision Measurements of the Coulombic Efficiency of Lithium-Ion Batteries and of Electrode Materials for Lithium-Ion Batteries. *J. Electrochem. Soc.*, **2010**, *157*, A196-A202.
(33) Bond, T. M.; Burns, J. C.; Stevens, D. A.; Dahn, H. M.; Dahn, J. R. Improving Precision and Accuracy in Coulombic Efficiency Measurements of Li-Ion Batteries. *J. Electrochem. Soc.*, **2013**, *160*, A521-A527.
(34) Sinha, N. N.; Marks, T. H.; Dahn, H. M.; Smith, A. J.; Coyle, D. J.; Dahn, J. J.; Dahn, J. R. The Rate of Active Lithium Loss from a Soft Carbon Negative Electrode as a Function of Temperature, Time and Electrode Potential. *J. Electrochem. Soc.,* **2012**, *159*, A1672-A1681.
(35) Petibon, R.; Rotermund, L.; Nelson, K. J.; Gozdz, A. S.; Xia, J.; Dahn, J. R. Study of Electrolyte Components in Li Ion Cells Using Liquid-Liquid Extraction and Gas Chromatography Coupled with Mass Spectrometry. *J. Electrochem. Soc.*, **2014**, *161*, A1167-A1172.
(36) Shirley, D. A. High-Resolution X-Ray Photoemission Spectrum of the Valence Bands of Gold. *Phys. Rev. B*, **1972**, *5*, 4709-4714.
(37) Zhuang, G. V.; Xu, K.; Yang, H.; Jow, T. R.; Ross Jr, P. N. Lithium Ethylene Dicarbonate Identified as the Primary Product of Chemical and Electrochemical Reduction of EC in 1.2 M $LiPF_6$/EC:EMC Electrolyte. *J. Phys. Chem. B.,* **2005,** *109*, 17567-17573.

(38) Xu, K.; Lam, Y.; Zhang, S. ; Jow, T. R.; Curtis, T. Solvation Sheath of Li^+ in Nonaqueous Electrolytes and Its Implication of Graphite/Electrolyte Interface Chemistry. *J. Phys. Chem. C.* **2007**, *111*,7411-7421.
(39) Burns, J. C.; Petibon, R.; Nelson, K. J.; Sinha, N. N.; Kassam, A.; Way, B. M.; Dahn, J. R. Studies of the Effect of Varying Vinylene Carbonate (VC) Content in Lithium Ion Cells on Cycling Performance and Cell Impedance. *J. Electrochem. Soc.*, **2013**, *160*, A1668-A1674.
(40) Burns, J. C.; Sinha, N. N.; Jain, G.; Ye, H.; VanElzen, C. M.; Lamanna, W. M.; Xiao, A.; Scott, E.; Choi, J.; Dahn, J. R. Impedance Reducing Additives and Their Effect on Cell Performance II. $C_3H_9B_3O_6$. *J. Electrochem. Soc.*, **2012**, *159*, A1105-A1113.
(41) Pantea, D.; Darmstadt, H.; Kaliaguine, S.; Sümmchen, L.; Roy, C. Electrical Conductivity of Thermal Carbon Blacks: Influence of Surface Chemistry. *Carbon*, **2001**, ***39***, 1147-1158.
(42) Pantea, D.; Darmstadt, H.; Kaliaguine, S.; Roy, C. Electrical Conductivity of Conductive Carbon Blacks: Influence of Surface Chemistry and Topology. *Applied Surface Science*, **2003**, *217*, 181-193.
(43) Aurbach, D.; Daroux, M. L.; Faguy, P. W.; Yeager, E. Identification of Surface Films Formed on Lithium in Propylene Carbonate Solutions. *J. Electrochem. Soc*., **1987**, *134*, 1611-A1620.
(44) Nie, M.; Chalasani, D.; Abraham, D. P.; Chen, Y.; Bose A.; Lucht, B. L. Lithium Ion Battery Graphite Solid Electrolyte Interphase Revealed by Microscopy and Spectroscopy. *J. Phys. Chem. C*, **2013**, *117*, 1257-1267.
(45) Dedryvère, R.; Gireaud, L.; Grugeon, S.; Laruelle, S.; Tarascon, J.-M., Gonbeau, D., Characterization of Lithium Alkyl Carbonates by X-ray Photoelectron Spectroscopy: Experimental and Theoretical Study. *J. Phys. Chem. B*, **2005**, *109*, 15868-15875.
(46) Malmgren, S.; Ciosek, K.; Hahlin, M.; Gustafsson, T.; Gorgoi, M.; Rensmo, H.; Edström, K. Comparing Anode and Cathode Electrode/Electrolyte Interface Composition and Morphology Using Soft and Hard X-ray Photoelectron Spectroscopy. *Electrochim. Acta*, **2013**, *97*, 23-32.
(47) Sloop, S.E.; Kerr, J.B.; Kinoshita, K. The role of Li-ion battery electrolyte reactivity in performance decline and self-discharge. *J. Power Sources*, **2003**, *119*, 330-337.
(48) Wang, Q.; Sun, J.; Yao, X.; Chen, C. Thermal Stability of $LiPF_6$/EC + DEC Electrolyte with Charged Electrodes for Lithium Ion Batteries. *Thermochim. Acta*, **2005**, *437*, 12-16.
(49) Gachot, G.: Grugeon, S.; Armand, M.; Pilard, S.; Guenot, P.; Tarascon, J.-M.; Laruelle, S. Deciphering the Multi-Step Degradation Mechanisms of Carbonate-Based Electrolyte in Li Batteries. *J. Power Sources*, **2008**, *178*, 409-421.
(50) Ismail, I.; Noda, A.; Nishimoto, A.; Watanabe, M. XPS Study of Lithium surface after contact with lithium-salt doped polymer electrolytes. *Electrochim. Acta*, **2001**, *46*, 1595-1603.
(51) Rendek, L. J.; Chottiner, G. S.; Scherson, D. A. The Reactivity of Linear Alkyl Carbonates toward Metallic Lithium. X-Ray Photoelectron Spectroscopy Studies in Ultrahigh Vacuum. *J. Electrochem. Soc*., **2002**, *149*, E408-E412.
(52) Kim, S.-P.; Van Duin, A.C.T.; Shenoy, V.B. Effect of Electrolytes on the Structure and Evolution of the Solid Electrolyte Interphase (SEI) in Li-Ion Batteries: A Molecular Dynamics Study. *J. Power Sources*, **2011**, *196*, 8590-8597.
(53) Philippe, B.; Dedryvère, R.; Allouche, J.; Lindgren, F.; Gorgoi, M.; Rensmo, H.; Gonbeau D.; Edström, K. Nanosilicon Electrodes for Lithium-Ion Batteries: Interfacial Mechanisms Studied by Hard and Soft X-ray Photoelectron Spectroscopy. *Chem. Mater*., **2012**, *24*, 1107-1115.
(54) Dedryvère, R.; Foix, D.; Franger, S.; Patoux, S.; Daniel, L.; Gonbeau, D., Electrode/Electrolyte Interface Reactivity in High-Voltage Spinel $LiMn_{1.6}Ni_{0.4}O_4/Li_4Ti_5O_{12}$ Lithium-Ion Battery. *J. Phys. Chem. C*, **2010**, *114*, 10999-11008.
(55) Bouayad, H.; Wang, Z.; Dupré, N.; Dedryvère, R.; Foix, D.; Franger, S.; Martin, J.-F.; Boutafa, L.; Patoux, S.; Gonbeau, D. *et al*. Improvement of Electrode/Electrolyte Interfaces in High-Voltage Spinel Lithium-Ion Batteries by Using Glutaric Anhydride as Electrolyte Additive. *J. Phys. Chem. C*, **2014**, *118*, 4634-4648.
(56) Aurbach, D. Nonaqueous Electrochemistry, *Marcel Dekker, Inc*., New York, **1999**.

(57) Ravdel, B.; Abraham, K.M.; Gitzendanner, R.; DiCarlo, J.; Lucht, B.; Campion, C. Thermal Stability of Lithium-Ion Battery Electrolytes. *J. Power Sources*, **2003**, *119*, 805-810.
(58) Edström, K.; Gustafsson, T.; Thomas, J. O. The Cathode–Electrolyte Interface in the Li-Ion Battery. *Electrochim. Acta*, **2004**, *50*, 397-403.
(59) Aurbach, D. Review of Selected Electrode–Solution Interactions which Determine the Performance of Li and Li Ion Batteries. *J. Power Sources*, **2000**, *89*, 206-218.
(60) Andersson, A. M.; Abraham, D. P.; Haasch, R.; MacLaren, S.; Liu, J.; Amine, K. Surface Characterization of Electrodes from High Power Lithium-Ion Batteries. *J. Electrochem. Soc*., **2002**, *149*, A1358-A1369.
(61) Ota, H. ; Akai, T.; Namita, H.; Yamaguchi, S.; Nomura, M. XAFS and TOF–SIMS Analysis of SEI Layers on Electrodes. *J. Power Sources*, **2003**, *119*, 567-571.